

Hydridorhodathiaboranes: Synthesis, Characterization, and Reactivity

Álvaro Álvarez,[†] Beatriz Calvo,[†] Ramón Macías,^{*,†} Fernando J. Lahoz,[†] and Luis A. Oro^{†,‡}

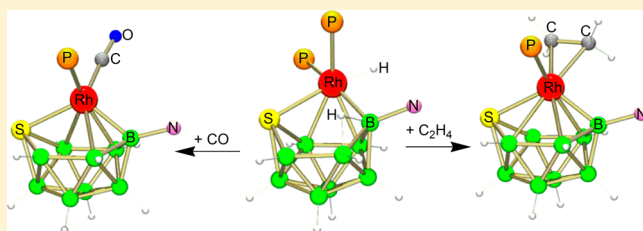
[†]Instituto de Síntesis Química y Catálisis Homogénea (ISQCH), Universidad de Zaragoza-Consejo Superior de Investigaciones Científicas, 50009-Zaragoza, Spain

[‡]Center of Research Excellence in Petroleum Refining and Petrochemicals, King Fahd University of Petroleum and Minerals (KFUPM), Dhahran 31261, Saudi Arabia

S Supporting Information

ABSTRACT: The reaction between pyridine and [8,8-(PPh₃)₂-*nido*-8,7-RhSB₉H₁₀] (**1**) has given the opportunity to synthesize a new family of 11-vertex hydridorhodathiaboranes that feature boron-bound N-heterocyclic ligands. To explore the scope of this reaction, **1** has been treated with the methylpyridine isomers (picolines) 2-Me-NC₅H₄, 3-Me-NC₅H₄, and 4-Me-NC₅H₄, affording the picoline ligated clusters [8,8,8-(H)(PPh₃)₂-9-(L)-*nido*-8,7-RhSB₉H₉], where L = 2-Me-NC₅H₄ (**3**), 3-Me-NC₅H₄ (**4**), 4-Me-NC₅H₄ (**5**).

Thermal treatment of these *nido* clusters leads to dehydrogenation and the formation of *isonido/closo*-[1,1-(PPh₃)₂-3-(L)-1,2-RhSB₉H₈] (**9–11**). Compounds **3–5** react with ethylene to form [1,1-(η^2 -C₂H₄)(PPh₃)₃-3-(L)-1,2-RhSB₉H₈] (**13–15**). Similarly, treatment of **3–5** with carbon monoxide produces [1,1-(CO)(PPh₃)₃-3-(L)-1,2-RhSB₉H₈] (**17–19**). These series of η^2 -C₂H₄ and CO ligated 11-vertex *isonido/closo*-rhodathiaboranes result from the substitution of one PPh₃ ligand by ethylene or CO together with H₂ loss and a concomitant *nido* to *closo/isonido* cluster structural transformation. The reactivity of **3–5** with propene, 1-hexene, and cyclohexene under a hydrogen atmosphere is also reported and compared with the reactivity of the pyridine ligated analogue [8,8,8-(H)(PPh₃)₂-9-(NC₅H₅)-*nido*-8,7-RhSB₉H₉] (**2**). Low-temperature NMR studies have allowed the characterization of intermediates which undergo inter- and intramolecular exchange processes, depending on the nature of the N-heterocyclic ligand. The CO ligand enhances the nonrigidity of the cluster, opening mechanisms of H₂ loss.



INTRODUCTION

The reactivity of metallocarboranes with organic molecules to give polyhedral clusters that feature metal–carbon bonds has been well studied.¹ In contrast, the organometallic chemistry of metallaboranes and metallaheteroboranes (containing p-block elements other than carbon in the cluster framework) has been less well developed.² There is a great potential for novel chemistry in this area that may be developed by a combination of the (oxidative and coordinative) flexibility of transition-metal centers together with the capability of boron-based clusters to exhibit redox flexibility in their classical *closo*–*nido*–*arachno*–*hypho* structural transformation.³ In other words, the synergic cooperation between a metal center and a (hetero)borane fragment can open new opportunities for bond activation and catalysis.

In the context of organometallic chemistry and catalysis based on metallaheteroboranes, we have focused our work on the 11-vertex rhodathiaborane [8,8-(PPh₃)₂-*nido*-8,7-RhSB₉H₁₀] (**1**).⁴ This polyhedral compound exhibits two principal points of reactivity: the metal center and an adjacent B–H unit on the pentagonal face (Scheme 1). Reactions with monodentate phosphines led to the formation of metal–ligand substitution products, [8,8-(PR₃)(PPh₃)₂-*nido*-8,7-RhSB₉H₁₀], as well as compounds resulting from the substitution of the

PPh₃ ligands and the addition of a third phosphine at the metal center, [8,8,8-(PR₃)₃-*nido*-8,7-RhSB₉H₁₀] (Scheme 1).⁵

Alternatively, the treatment of **1** with pyridine affords a hydridorhodathiaborane, [8,8,8-(H)(PPh₃)₂-9-(NC₅H₅)-*nido*-8,7-RhSB₉H₉] (**2**), in which the pyridine ligand binds to boron-9 adjacent to the metal on the pentagonal face (Scheme 1).⁶

The bis-PPh₃ ligated 11-vertex *nido*-rhodathiaborane **1** also undergoes substitution reactions with 1,3-dimethylimidazol-2-ylidene (IME), giving a mixture that contains the products of monosubstitution and disubstitution, [8,8-(PPh₃)(IME)-*nido*-8,7-RhSB₉H₁₀] and [8,8-(IME)₂-*nido*-8,7-RhSB₉H₁₀] (Scheme 1).⁷ The treatment of the monosubstituted carbene ligated *nido*-rhodathiaborane with pyridine affords a new *isonido* cluster, [1,1-(IME)(PPh₃)₃-3-(NC₅H₅)-*isonido*-8,7-RhSB₉H₈], formed by pyridine-cage substitution and dihydrogen loss. Interestingly, the bis-carbene ligated analogue does not react with pyridine.

These results demonstrate that compounds **1** and **2** are versatile clusters that can be easily prepared and systematically modified at the rhodium center by substitutional chemistry.

Received: April 9, 2014

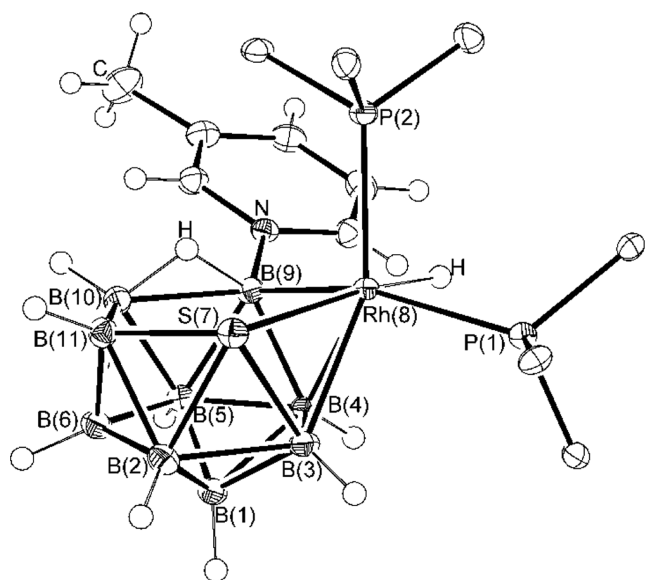


Figure 1. Molecular structure of **4**. Only the *ipso* carbon atoms on the phenyl groups are included to aid clarity. Ellipsoids are shown at the 50% probability level.

between skeletal electron pairs and structure has been dealt with previously in detail.¹³

Table 1 gathers selected distances and angles for compounds **2** and **4–6**. Overall, there are no substantial differences among intramolecular distances and angles in these series of hydridorhodathiaboranes. It is noteworthy, however, that the 3-picoline derivative **4** exhibits the longest Rh–P distance at 2.3752(8) Å, perhaps due to steric interactions between the methyl group at position 3 in the N-heterocyclic ring and the bulky PPh₃ ligands. In all of the clusters except for **5**, the longest Rh–P distance corresponds to the phosphine ligand that is trans to boron-9, substituted with the pyridinic ligand,

suggesting a stronger structural trans influence in comparison to the B(3)–B(4) edge to which the other phosphine, P(2), lies trans. The shorter Rh–P distances found in the bis-PMePh₂ derivative **6** agree well with the fact that methyl-diphenylphosphine is a better σ -donor ligand than PPh₃.

It is well-known that the boron vertices of metal-face-bound carborane ligands have a larger trans influence than the cage carbon atoms.¹⁴ This fact is important because it implies that the most stable metal-to-carborane exopolyhedral ligand orientation is that in which the strongest structural trans effect ligands on the metal lie effectively trans to the carbon atoms. This may be extended to metallathiaboranes where the metal-bound sulfur atoms also have a lower trans influence than the boron atoms in the face of the metal-to-thiaborane linkage. Thus, in the hydridorhodathiaboranes **2–6**, the hydride ligand lies trans to the sulfur vertex. The same kind of exopolyhedral ligand control has been observed in other metallathiaboranes that bear hydride ligands.¹⁵ Moreover, in some 11-vertex *nido*-rhodathiaboranes, it has been calculated that a metal–thiaborane interaction change from a sulfur–metal–hydride trans arrangement to a boron–metal–hydride trans configuration can have an energy cost as high as 12 kcal/mol.^{12,16}

¹¹B and ¹H NMR data for compounds **3–5** are given in Table 2; and Figure 2 compares the ¹¹B spectra of the 2- and 3-picoline ligated clusters **3** and **4** with those of the previously reported pyridine analogues **2** and [8,8,8-(H)(PMe₃)(PPh₃)-9-(NC₅H₅)-*nido*-8,7-RhSB₉H₉] (**7**). These *nido*-hydridorhodathiaboranes show nine resonances in the interval between δ_B +15 and –30 ppm, in agreement with an asymmetric molecular structure in solution. The spectra among the clusters are remarkably similar, with the only noticeable deviation corresponding to the B(10) resonance of the 2-picoline derivative, which is deshielded by about 4 ppm from the general trend (Figure 2).

The ¹H{¹¹B} NMR spectra of **3–5** show a broad singlet and an apparent quartet in the high-field region, assigned to the

Table 1. Selected Interatomic Distances (Å) and Angles (deg) between Interatomic Vectors with Standard Uncertainties (su) in Parentheses for [8,8,8-(H)(PPh₃)₂-9-(NC₅H₄)-*nido*-8,7-RhSB₉H₉] (**2**), [8,8,8-(H)(PPh₃)₂-9-(3-Me-NC₅H₄)-*nido*-8,7-RhSB₉H₉] (**4**), [8,8,8-(H)(PPh₃)₂-9-(4-Me-NC₅H₄)-*nido*-8,7-RhSB₉H₉] (**5**), and [8,8,8-(H)(PMePh₂)₂-9-(NC₅H₄)-*nido*-8,7-RhSB₉H₉] (**6**)

	2 ^a	4	5	6 ^b
Rh(8)–S(7)	2.431(2)	2.4132(8)	2.4373(14)	2.4270(5)
Rh(8)–P(1)	2.354(2)	2.3752(8)	2.3488(14)	2.3224(6)
Rh(8)–P(2)	2.341(2)	2.3383(7)	2.3560(14)	2.3091(6)
Rh(8)–B(3)	2.201(10)	2.235(3)	2.239(6)	2.230(2)
Rh(8)–B(4)	2.217(11)	2.236(3)	2.216(5)	2.209(2)
Rh(8)–B(9)	2.220(9)	2.208(3)	2.210(6)	2.214(2)
S(7)–B(2)	1.980(9)	1.991(3)	1.984(6)	1.996(3)
S(7)–B(3)	2.059(11)	2.085(3)	2.041(6)	2.060(3)
S(7)–B(11)	1.953(9)	1.909(3)	1.943(6)	1.928(3)
N(1)–B(9)	1.547(11)	1.569(3)	1.555(7)	1.556(3)
B(6)–B(11) (shortest)	1.727(14)	1.738(4)	1.741(8)	1.748(4)
B(2)–B(3) (longest)	1.906(14)	1.902(4)	1.915(9)	1.913(4)
B(9)–B(10)	1.856(14)	1.868(4)	1.870(8)	1.874(3)
P(1)–Rh(8)–P(2)	100.27(7)	101.68(3)	101.77(5)	98.10(2)
S(7)–Rh(8)–P(1)	96.38(7)	103.16(3)	96.81(5)	97.82(2)
S(7)–Rh(8)–P(2)	102.05(8)	97.63(3)	101.03(5)	105.080(19)
Rh(8)–B(9)–N(1)	120.6(5)	120.81(16)	121.6(4)	119.30(15)
S(7)–Rh(8)–B(9)	87.1(3)	88.17(7)	88.02(15)	87.79(6)
P(1)–Rh(8)–B(9)	162.4(3)	157.80(8)	159.02(15)	163.22(6)
P(2)–Rh(8)–B(9)	95.8(3)	95.54(8)	97.28(15)	95.66(6)

Table 2. ^{11}B and ^1H NMR Data for $[\text{8,8,8-(H)(PPh}_3)_2\text{-9-(2-Me-NC}_5\text{H}_4)\text{-nido-8,7-RhSB}_9\text{H}_9]$ (**3**), $[\text{8,8,8-(H)(PPh}_3)_2\text{-9-(3-Me-NC}_5\text{H}_4)\text{-nido-8,7-RhSB}_9\text{H}_9]$ (**4**), and $[\text{8,8,8-(H)(PPh}_3)_2\text{-9-(4-Me-NC}_5\text{H}_4)\text{-nido-8,7-RhSB}_9\text{H}_9]$ (**5**) in CD_2Cl_2 Compared to the Corresponding DFT/GIAO-Calculated ^{11}B Nuclear Shielding Values Calculated for the PH_3 Models (in Brackets)

assignt ^a	3		4		5	
	$\delta(^{11}\text{B})$	$\delta(^1\text{H})^b$	$\delta(^{11}\text{B})$	$\delta(^1\text{H})^b$	$\delta(^{11}\text{B})$	$\delta(^1\text{H})^b$
9 ^c	+11.1 [+18.8]	2-Me-NC ₅ H ₄	+12.1 [+17.9]	3-Me-NC ₅ H ₄	+11.8 [+17.6]	4-Me-NC ₅ H ₄
3	+6.1 ^d [+8.5]	+3.42	+8.1 [+8.9]	+3.51	+7.8 ^e [+9.4]	+3.53
6	+4.0 [+5.5]	+3.03	+3.9 [+7.5]	+2.60	+3.3 [+7.4]	+2.63
11	+1.5 [+2.1]	+3.58	+0.6 [+2.2]	+4.13	+0.2 ^f [+2.2]	+4.13
4	-3.9 [+1.9]	+3.26	-3.7 [-0.1]	+2.85	-3.8 [-0.1]	+2.85
5	-12.1 ^g [-14.0]	+1.93	-10.0 ^h [-11.1]	+1.83	-10.2 ⁱ [-10.7]	+1.81
10	-14.4 [-19.2]	+1.06	-17.9 [-22.7]	+0.92	-17.9 [-23.0]	+0.88
1	-25.0 ^j [-23.8]	+1.49	-25.6 [-25.4]	+1.50	-25.7 [-25.1]	+1.49
2	-27.2 [-27.9]	+1.21	-29.1 [-28.5]	+1.11	-28.5 [-28.4]	+1.09
$\mu(9, 10)$		-0.95		-1.38		-1.42
Rh(8)-H		-12.49 ^k		-12.47 ^l		-12.43 ^m

^aAssignments based on $^1\text{H}\{^{11}\text{B}\}$ selective experiments and DFT calculations. ^bProton chemical shifts corresponding to boron-bound hydrogen atoms. ^cPicoline-substituted vertex. ^d $^1J(^{11}\text{B}-^1\text{H}) = 132$ Hz. ^e $^1J(^{11}\text{B}-^1\text{H}) = 112$ Hz. ^f $^1J(^{11}\text{B}-^1\text{H}) = 127$ Hz. ^g $^1J(^{11}\text{B}-^1\text{H}) = 142$ Hz. ^h $^1J(^{11}\text{B}-^1\text{H}) = 140$ Hz. ⁱ $^1J(^{11}\text{B}-^1\text{H}) = 137$ Hz. ^j $^1J(^{11}\text{B}-^1\text{H}) = 146$ Hz. ^k $^1J(^{11}\text{B}-^1\text{H}) = 150$ Hz. ^lApparent quartet: $^1J(^{103}\text{Rh}-^1\text{H}) + ^2J(^{31}\text{P}_\text{A}-^1\text{H}) + ^2J(^{31}\text{P}_\text{B}-^1\text{H}) \approx 17$ Hz. ^mApparent quartet: $^1J(^{103}\text{Rh}-^1\text{H}) + ^2J(^{31}\text{P}_\text{A}-^1\text{H}) + ^2J(^{31}\text{P}_\text{B}-^1\text{H}) \approx 20$ Hz; $^1\text{H}\{^{31}\text{P}\}$ δ -12.43 (d, $^1J(^{103}\text{Rh}-^1\text{H}) = 19.7$ Hz, H).

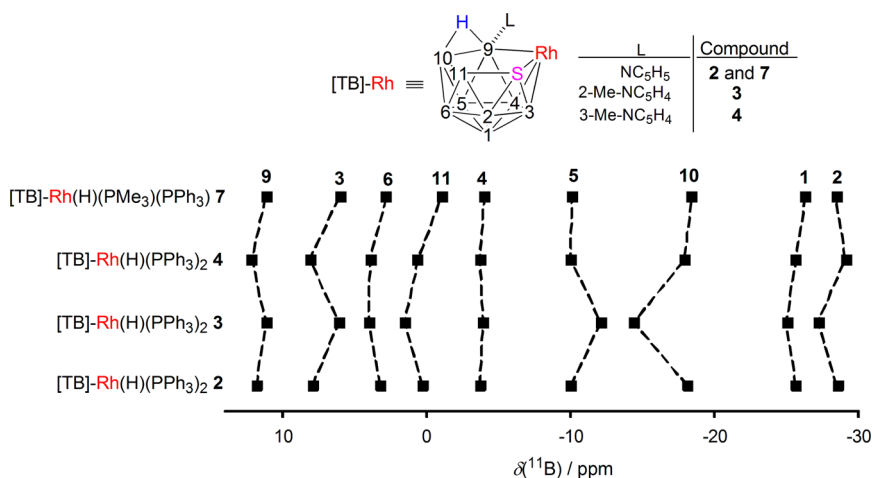


Figure 2. Representation of the ^{11}B NMR spectra of **2–4** and **7**. Hatched lines connect equivalent positions. Assignments made on the basis of DFT calculations.

$\text{B}(9)\text{--B}(10)$ bridging hydrogen atom and to the $\text{Rh}\text{--H}$ hydride ligand, respectively. Thus, these spectroscopic data can be taken as diagnostic for the formation of these 11-vertex *nido*-hydridorhathiorboranes. In this regard, it is interesting to note that the $\text{B}(9)\text{--H--B}(10)$ bridging proton resonance of the 2-picoline derivative ($\delta_{\text{H}} -0.95$ ppm) features a significant shift toward low frequency from the mean value of $\delta_{\text{H}} -1.28$ ppm that has been found in the series of picoline ligated *nido* clusters reported here, as well as the previously reported hydrido-rhathiorborane counterparts of general formulation $[\text{8,8,8-(H)(PR}_3)_2\text{-9-(NC}_5\text{H}_5)\text{-nido-8,7-RhSB}_9\text{H}_9]$, where $\text{PR}_3 = \text{PPh}_3$ (**2**), PMePh_2 (**6**), PPh_3 and PMe_3 (**7**), PPhMe_2 , or PPh_3 and PMe_2Ph .⁹

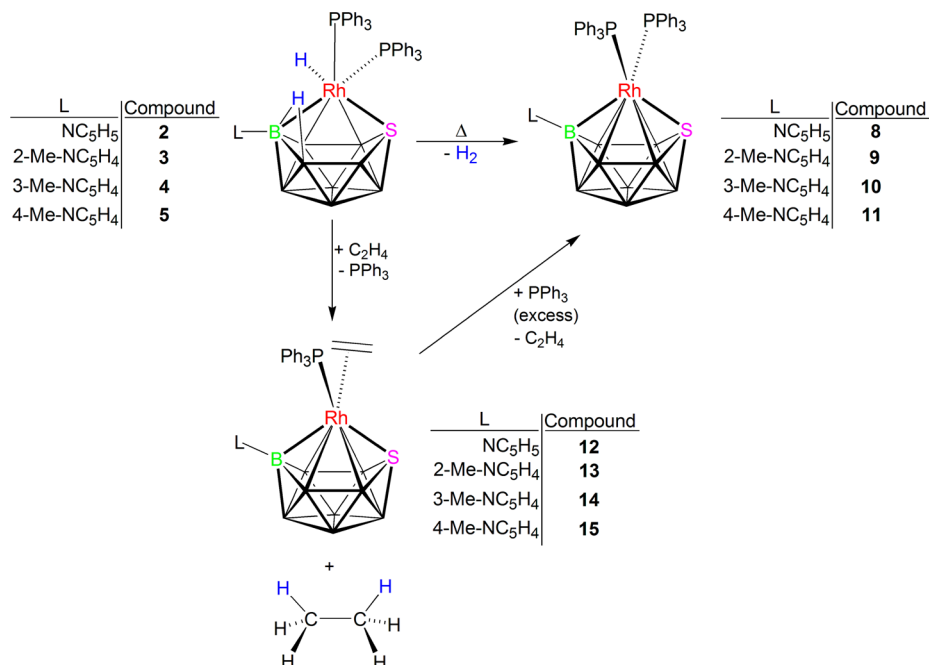
The lower conformational freedom of the 2-picoline substituent around the $\text{B}(3)\text{--N}$ bond in comparison to pyridine and 3- and 4-picolines may be the cause of the shift to higher frequency of the $\text{B}(9)\text{--H--B}(10)$ bridging proton resonance.

The $^{31}\text{P}\{^1\text{H}\}$ NMR spectra of **3–5** exhibit two doublets of doublets at low temperature, the signal at the highest frequency

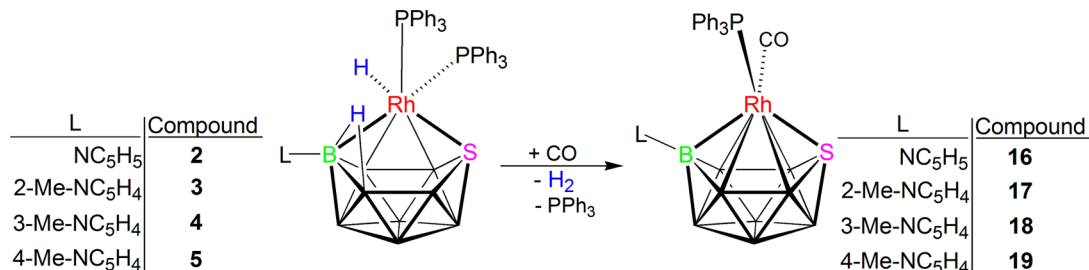
being significantly broader. This latter resonance broadens and shifts to low frequency as the temperature increases, whereas the low-frequency signal moves slightly to higher frequency. This variable-temperature NMR behavior is illustrated in Figure S1 for compound **5**: from low to high temperatures, the two resonances broaden and cross each other. Similar changes were first reported for the pyridine analogue **2**.^{6a}

It has been proposed that the temperature-dependent broadening in the $^{31}\text{P}\{^1\text{H}\}$ spectra of pyridine ligated hydridorhathiorboranes $[\text{8,8,8-(H)(PR}_3)_2\text{-9-(NC}_5\text{H}_5)\text{-nido-RhSB}_9\text{H}_9]$ may arise mainly from the effects of “thermal decoupling” on the boron nuclei,¹⁷ together with the dissociation of the phosphine ligand trans to $\text{B}(9)$.^{6b,9} On this rationale, the broader peak at high frequency in this new family of 11-vertex hydrido ligated clusters may be assigned to the phosphine ligand that is trans to the picoline-substituted boron vertex at the 9-position.

Studies of Reactivity. Thermal and Chemical Cluster Dehydrogenations. The hydridorhathiorboranes **3–5** are stable in solution at room temperature. However, heating at

Scheme 3. Reactivity of 2–5: Thermal Dehydrogenation and Reactions with C₂H₄

Scheme 4. Reactions of 2–5 with Carbon Monoxide



reflux temperature in dichloromethane results in the loss of H₂, yielding the corresponding *closo/isonido* clusters [1,1-(PPh₃)₂-3-(L)-1,2-RhSB₉H₈], where L = 2-Me-NC₅H₄ (**9**), 3-Me-NC₅H₄ (**10**), 4-Me-NC₅H₄ (**11**) (Scheme 3).

The picoline ligated rhodathiaboranes **2–5** react with ethylene to give the corresponding *closo/isonido* clusters, [1,1-(η^2 -C₂H₄)(PPh₃)₂-3-(L)-1,2-RhSB₉H₈] (**13–15**). In these reactions, we have also observed formation of ethane.

The η^2 -C₂H₄ ligand in these 11-vertex *closo/isonido* clusters is labile, and it can be substituted by PPh₃ to give the corresponding bis-PPh₃ ligated derivatives (Scheme 3). In fact, this route is more appropriate for the synthesis of the *closo/isonido* compounds **8–11** than the thermal dehydrogenation of the hydride *nido* clusters **2–5**.

The reactivity of compounds **2** and **3** has been also explored with other alkenes. Thus, the pyridine ligated cluster **2** reacts slowly with propylene at room temperature, and after 4 days of stirring the result is a mixture that contains propane together with the starting reagent **2** (35%) and its dehydrogenation product **8** (65%). The reaction with 1-hexene, after 3 days, afforded 1-hexene (75%), 2-hexene (17%), 3-hexene (7%), and 1-hexane (1%). Under the same conditions, compound **2** did not react with cyclohexene.

In the case of the 2-picoline analogue **3** after 1 h the reaction with propylene affords the bis-PPh₃ *closo* derivative **9** and formation of propane. Reaction with 1-hexene, after 1 day, gave

a mixture composed of 1-hexene (63%), 2-hexene (34%), and 1-hexane (3%). Moreover, **3** reacted with cyclohexene to give 2% of cyclohexane after 1 day. These results demonstrate that the 2-picoline derivative **3** is more reactive with alkenes than the pyridine analogue **2** and that the reaction products are the result of the hydrogenation and isomerization of the double bonds (in the case of 1-hexene).

In a fashion similar to the reactions with ethylene, the treatment of these pyridine- and picoline ligated hydridorhodathiaboranes **2–5** with carbon monoxide affords the products of hydrogen loss and PPh₃ substitution, [1,1-(CO)(PPh₃)₂-3-(L)-1,2-RhSB₉H₈], (**17–19**) (Scheme 4).^{6a}

It should be noted that the reactivity of the picoline ligated hydridorhodathiaboranes **3–5** with carbon monoxide and with ethylene, reported here, reproduces the results previously reported for the pyridine ligated analogue **2**.^{6b}

As we can see, thermal dehydrogenation and reactions with CO and C₂H₄ are convenient routes to the synthesis of 11-vertex rhodathiaboranes with *closo/isonido* cluster geometries, which bear different exopolyhedral ligands at either the metal center or the boron-3 vertex. Thus, these reactions broaden the scope of the substitution chemistry in this system, allowing a systematic tuning of their reactivity.

All of the new 11-vertex *isonido* clusters **9–11**, **13–15**, and **17–19** have been characterized by NMR spectroscopy, and the data are gathered in Tables 3–5. A comparison of the ¹¹B NMR

Table 3. ^{11}B and ^1H NMR Data for [1,1-(PPh₃)₂-3-(NC₅H₅)-isonido-1,2-RhSB₉H₉] (8), [1,1-(PPh₃)₂-3-(2-Me-NC₅H₄)-closo-1,2-RhSB₉H₈] (9), [1,1-(PPh₃)₂-3-(3-Me-NC₅H₄)-closo-1,2-RhSB₉H₈] (10), and [1,1-(PPh₃)₂-3-(4-Me-NC₅H₄)-closo-1,2-RhSB₉H₈] (11) in CD₂Cl₂ Compared to the Corresponding DFT/GIAO-Calculated ^{11}B Nuclear Shielding Values (in Brackets)

assign ^a	8 ^{6b}		9		10		11	
	$\delta(^{11}\text{B})$	$\delta(^1\text{H})^b$	$\delta(^{11}\text{B})$	$\delta(^1\text{H})^b$	$\delta(^{11}\text{B})$	$\delta(^1\text{H})^b$	$\delta(^{11}\text{B})$	$\delta(^1\text{H})^b$
3 ^c	+54.6 [+58.4]	NC ₅ H ₅	+53.3 [+57.8]	2-Me-NC ₅ H ₄	+54.8 [+59.0]	3-Me-NC ₅ H ₄	+54.9 [+59.5]	4-Me-NC ₅ H ₄
9	+27.3 ^d [+30.1]	+4.09	+25.4 [+29.7]	+4.32	+27.5 [+30.2]	+4.24	+27.3 ^e [+29.6]	+4.09
4, 5	-0.5 [+6.7, +5.4]	+1.27	-0.6 [+10.8, +3.1]	+1.27	+0.5 [+7.9, +4.1]	+1.28	-0.7 [+8.4, +3.4]	+1.29 (2H)
8	-15.2 [-12.2]	+2.16	-14.2 [-13.1]	+2.40	-14.3 [-12.6]	+2.37	-15.5 [-12.9]	+2.17
6, 7	-24.2 ^f [-18.1, -21.8]	-0.22 (2H)	-21.9 [-15.4, -23.0]	+0.05 (4H)	-23.8 [-14.8, -22.4]	-0.10 (2H)	-24.6 [-14.1, -22.0]	-0.23 (4H)
10, 11	-34.4 ^g [-29.3, -29.6]	-0.27 (2H)	-29.8 [-26.5, -31.1]		-29.9 [-28.8, -29.5]	-0.29 (2H)	-30.7 [-28.0, -29.7]	

^aAssignments based on $^1\text{H}\{^{11}\text{B}\}$ selective experiments and DFT calculations. ^bProton chemical shifts corresponding to boron-bound hydrogen atoms. ^cPicoline-substituted vertex. ^d $^dJ(^{11}\text{B}-^1\text{H}) = 144$ Hz. ^e $^eJ(^{11}\text{B}-^1\text{H}) = 137$ Hz. ^f $^fJ(^{11}\text{B}-^1\text{H}) = 129$ Hz. ^g $^gJ(^{11}\text{B}-^1\text{H}) = 139$ Hz.

Table 4. ^{11}B and ^1H NMR Data for [1,1-(PPh₃)(η^2 -C₂H₄)-3-(NC₅H₅)-isonido-1,2-RhSB₉H₈] (12), [1,1-(PPh₃)(η^2 -C₂H₄)-3-(2-Me-NC₅H₄)-closo-1,2-RhSB₉H₈] (13), [1,1-(PPh₃)(η^2 -C₂H₄)-3-(3-Me-NC₅H₄)-closo-1,2-RhSB₉H₈] (14), and [1,1-(PPh₃)(η^2 -C₂H₄)-3-(4-Me-NC₅H₄)-closo-1,2-RhSB₉H₈] (15) in CD₂Cl₂ Compared to the Corresponding DFT/GIAO-Calculated ^{11}B Nuclear Shielding Values (in Brackets)

assign ^a	12 ^{6a}		13		14		15	
	$\delta(^{11}\text{B})$	$\delta(^1\text{H})^b$	$\delta(^{11}\text{B})$	$\delta(^1\text{H})^b$	$\delta(^{11}\text{B})$	$\delta(^1\text{H})^b$	$\delta(^{11}\text{B})$	$\delta(^1\text{H})^b$
3 ^c	+55.7 [+58.5]	NC ₅ H ₅	+54.9	2-Me-NC ₅ H ₄	+56.3	3-Me-NC ₅ H ₄	+55.3	4-Me-NC ₅ H ₄
9	+26.4 ^d [+28.5]	+4.36	+24.9 ^e	+4.27	+26.2 ^f	+4.22	+26.2 ^g	+4.33
5	+0.8 [+9.0]	+1.80	+4.0	+2.01	+1.4	+1.93	+0.1	+2.05
4	-0.1 [+4.2]	+2.06	-1.1	+1.58	-0.1	+1.65	-0.7	+1.72
8	-14.5 [-13.3]	+2.46	-14.1	+2.53	-14.6	+2.30	-15.3	+2.45
7	-22.2 [-16.8]	+0.54	-20.4	+0.87	-22.6	+0.37	-22.5	+0.39
6	-24.6 [-22.0]	-0.17	-25.4 ^h	-0.54	-24.6	-0.23	-25.1	-0.23
10, 11	-30.3 [-27.4, -27.0]	+0.42, -0.01	-29.1, -29.8	+0.23, -0.10	-30.0, -30.7	+0.19, -0.21	-30.0	+0.53, -0.01

^aAssignments based on $^1\text{H}\{^{11}\text{B}\}$ selective experiments and DFT calculations. ^bProton chemical shifts corresponding to boron-bound hydrogen atoms. ^cPicoline-substituted vertex. ^d $^dJ(^{11}\text{B}-^1\text{H}) = 124$ Hz. ^e $^eJ(^{11}\text{B}-^1\text{H}) = 127$ Hz. ^f $^fJ(^{11}\text{B}-^1\text{H}) = 124$ Hz. ^g $^gJ(^{11}\text{B}-^1\text{H}) = 127$ Hz. ^h $^hJ(^{11}\text{B}-^1\text{H}) = 134$ Hz.

Table 5. ^{11}B and ^1H NMR Data for [1,1-(PPh₃)(CO)-9-(NC₅H₅)-closo-1,2-RhSB₉H₉] (16), [1,1-(PPh₃)(CO)-3-(2-Me-NC₅H₄)-closo-1,2-RhSB₉H₈] (17), [1,1-(PPh₃)(CO)-3-(3-Me-NC₅H₄)-closo-1,2-RhSB₉H₈] (18), and [1,1-(PPh₃)(CO)-3-(4-Me-NC₅H₄)-closo-1,2-RhSB₉H₈] (19) in CD₂Cl₂ Compared to the Corresponding DFT/GIAO-Calculated ^{11}B Nuclear Shielding Values (in Brackets)

assign ^a	16 ^{6b}		17		18		19	
	$\delta(^{11}\text{B})$	$\delta(^1\text{H})^b$	$\delta(^{11}\text{B})$	$\delta(^1\text{H})^b$	$\delta(^{11}\text{B})$	$\delta(^1\text{H})^b$	$\delta(^{11}\text{B})$	$\delta(^1\text{H})^b$
3 ^c	+55.4 [+59.5]	NC ₅ H ₅	+53.8 [+57.7]	2-Me-NC ₅ H ₄	+55.7 [+59.7]	3-Me-NC ₅ H ₄	+55.3 [+58.7]	4-Me-NC ₅ H ₄
9	+28.1 ^d [+30.4]	+4.34	+27.4 ^e [+29.2]	+4.34	+28.2 ^f [+30.1]	+4.33	+28.2 [+29.7]	+4.44
5	+1.1 [+8.9]	+2.39	+0.97 (2B) [+14.2, +0.8]	+2.40	+1.2 [+8.8]	+2.40	+1.5 [+12.2]	+2.50
4	-0.7 [+4.2]	+1.08		+1.33	-0.7 [+4.2]	+1.12	-0.5 [+1.3]	+1.21
8	-14.4 [-13.4]	+2.37	-13.6 [-14.3]	+2.40	-14.7 [-13.6]	+2.40	-14.4 [-14.4]	+2.50
6	-24.4 [-17.1]	+0.66	-22.9 [-17.2]	+0.73	-24.9 [-17.1]	+0.65	-24.5 [-17.3]	+0.68
7	-26.1 [-21.8]	-0.08	-24.9 [-22.9]		-26.1 [-21.6]	+0.03	-25.9 [-24.1]	+0.22
10, 11	-31.9 ^g	+0.07, 0.00	-31.8 ^h [-24.0, -30.6]	+0.01 (3H)	-32.0 [-26.8, -29.3]	-0.01 (2H)	-31.9 ⁱ [-25.9, -29.7]	+0.15 (2H)

^aAssignments based on $^1\text{H}\{^{11}\text{B}\}$ selective experiments and DFT calculations. ^bProton chemical shifts corresponding to boron-bound hydrogen atoms. ^cPicoline-substituted vertex. ^d $^dJ(^{11}\text{B}-^1\text{H}) = 118$ Hz. ^e $^eJ(^{11}\text{B}-^1\text{H}) = 129$ Hz. ^f $^fJ(^{11}\text{B}-^1\text{H}) = 133$ Hz. ^g $^gJ(^{11}\text{B}-^1\text{H}) = 127$ Hz. ^h $^hJ(^{11}\text{B}-^1\text{H}) = 138$ Hz. ⁱ $^iJ(^{11}\text{B}-^1\text{H}) = 142$ Hz. ^j $^jJ(^{11}\text{B}-^1\text{H}) = 138$ Hz.

spectra corresponding to the pyridine derivative **8** and the 2-picoline derivatives **9**, **13**, and **17** is depicted in Figure 3. The patterns are very similar within this series of 11-vertex *closo*/*isonido* clusters, suggesting that changes between the

exopolyhedral ligands, either at the metal or at the boron vertex, do not substantially affect the overall shielding of the boron cage nuclei.

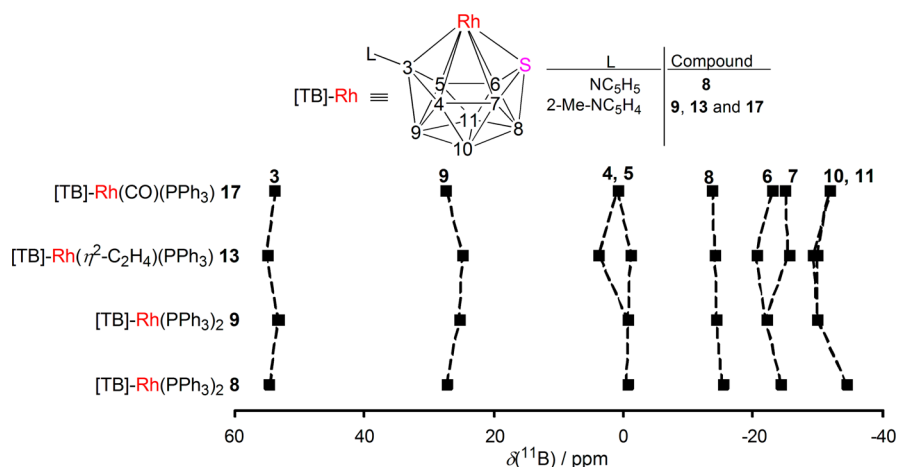


Figure 3. Diagram that represents the chemical shifts in the ^{11}B NMR spectra of **8**, **9**, **13**, and **17**. Hatched lines connect equivalent positions. Assignments are based on DFT GIAO calculations.

The $^{31}\text{P}\{^1\text{H}\}$ NMR spectra of the *closo/isonido* derivatives **8**–**19** show doublets at room temperature. It is of interest to note that, as the temperature decreases, the broad doublet of the 2-picoline derivative **9** broadens further and splits into two broad doublets. This variable-temperature behavior demonstrates that the cluster is undergoing a fluxional process. A plausible mechanism that could rationalize this intramolecular rearrangement is a hindered rotation of the 2-picoline ligand around the N–B(3) bond, rendering the exopolyhedral PPh_3 ligands at the rhodium center nonequivalent (Scheme 5). The free energy of activation, ΔG^\ddagger_{273} , measured at the coalescence temperature is 12 kcal/mol.

Scheme 5. Hindered Rotation of the 2-Picoline Ligand around the B(3)–N Bond in Compound 9

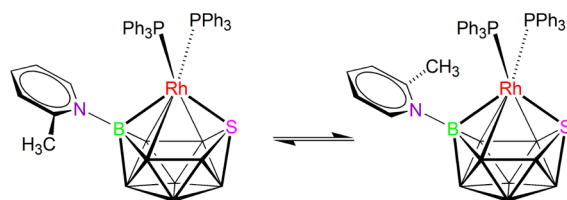


Table 6 gathers the IR CO stretching frequencies of the CO ligated *closo/isonido* clusters **16**–**19**. The frequencies are similar

Table 6. Measured and Calculated IR Stretching Frequencies

compd	ν_{CO} (cm^{-1})	
	exptl	calcd ^a
[1,1-(CO)(PPh ₃)-3-(NC ₅ H ₅)-1,2-RhSB ₉ H ₈] (16)	1980	1903
[1,1-(CO)(PPh ₃)-3-(2-Me-NC ₅ H ₄)-1,2-RhSB ₉ H ₈] (17)	1982	1905
[1,1-(CO)(PPh ₃)-3-(3-Me-NC ₅ H ₄)-1,2-RhSB ₉ H ₈] (18)	1974	1898
[1,1-(CO)(PPh ₃)-3-(4-Me-NC ₅ H ₄)-1,2-RhSB ₉ H ₈] (19)	1985	1911

^aThe computed carbonyl frequencies were scaled with a 0.9613 factor.¹⁸

within the series, with the smallest value corresponding to the 3-picoline derivative. The DFT-calculated values are around 76 cm^{-1} smaller than the measured data, and they follow the experimental trend. Decreasing CO frequency is an accepted measure of increasing negative charge buildup on the metal center. Hence, it appears that the substitution of boron-3 with

the N-heterocyclic ligands studied herein does not lead to a significant charge difference at the metal center.

The 2-picoline ligated cluster **9** has been characterized by X-ray crystallography (Figure 4). Table 7 gives selected distances

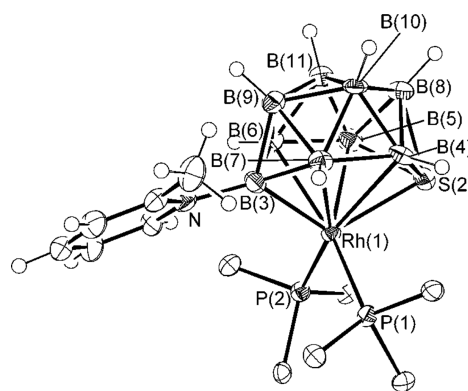


Figure 4. Molecular structure of [1,1-(PPh₃)₂-3-(2-Me-NC₅H₄)-*closo*-1,2-RhSB₉H₈] (**9**). Only the *ipso* carbon atoms on the phenyl groups are included to aid clarity. Ellipsoids are shown at the 50% probability level.

and angles for this derivative and, to help in comparison, for the pyridine ligated analogues [1,1-(PR₃)₂-3-(NC₅H₅)-1,2-RhSB₉H₈], where PR₃ = PPh₃ (**8**), PMe₃ and PPh₃ (**20**), or PMe₂Ph (**21**). At first sight, the structures all look like 11-vertex *closo* clusters based on an octadecahedron. It should be noted that the clusters exhibit long Rh(1)–B(5) distances close to 2.5 Å, which is the upper limit normally considered as bonding. In the case of compound **8**, the distance 2.562(6) Å is outside this limit. This elongation results in the formation of a pseudo-square open face that is a structural feature common in *closo* 11-vertex clusters,¹⁹ which represent intermediates along the structural continuum from *closo* to *nido*.^{16,20}

Reactions with CO at Low Temperatures. In the previous section, it was mentioned that the reaction of 11-vertex rhodathiaboranes with carbon monoxide affords the products of dihydrogen loss and the substitution of one of the PPh₃ ligands by CO. These reactions are quantitative when carried out at room temperature for periods on the order of hours. However, short reaction times and low-temperature NMR studies have allowed the characterization of intermediates that provide new

Table 7. Selected Interatomic Distances (Å) and Angles (deg) between Interatomic Vectors with Standard Uncertainties (su) in Parentheses for [1,1-(PPh₃)₂-3-(NC₅H₅)-*isonido*-8,7-RhSB₉H₉] (8), [1,1-(PPh₃)₂-3-(2-Me-NC₅H₄)-*closo*-8,7-RhSB₉H₈] (9), [1,1-(PPh₃)(PMe₃)-3-(NC₅H₅)-*closo*-8,7-RhSB₉H₈] (20), and [1,1-(PMe₂Ph)₂-3-(NC₅H₅)-*closo*-8,7-RhSB₉H₈] (21)

	8 ¹⁰	9	20	21
Rh(1)–S(2)	2.3997(14)	2.3885(14)	2.3841(9)	2.3826(11)
Rh(1)–P(1)	2.3278(13)	2.3276(15)	2.2889(10) [PMe ₃]	2.2821(11)
Rh(1)–P(2)	2.3012(12)	2.3243(15)	2.2710(9) [PPh ₃]	2.2741(11)
Rh(1)–B(3)	2.085(6)	2.119(7)	2.087(4)	2.067(4)
Rh(1)–B(4)	2.400(6)	2.435(7)	2.401(4)	2.362(5)
Rh(1)–B(5)	2.562(6)	2.485(7)	2.471(4)	2.487(5)
Rh(1)–B(6)	2.344(6)	2.364(7)	2.380(4)	2.333(4)
Rh(1)–B(7)	2.387(6)	2.372(7)	2.354(4)	2.409(5)
S(2)–B(4)	1.918(6)	1.934(8)	1.953(4)	1.932(5)
S(2)–B(5)	1.956(6)	1.921(7)	1.937(4)	1.969(5)
S(2)–B(8)	1.989(6)	2.001(7)	1.999(5)	1.989(5)
N–B(3)	1.532(8)	1.556(7)	1.546(5)	1.541(5)
B(3)–B(7) (shortest)	1.709(8)	1.716(10)	1.705(5)	1.712(6)
B(4)–B(8) (longest)	1.893(9)	1.905(10)	1.917(6)	1.916(7)
P(1)–Rh(1)–P(2)	96.97(4)	97.86(5)	96.68(4)	96.27(4)
P(1)–Rh(1)–S(2)	102.32(5)	107.75(5)	103.17(4)	103.77(4)
P(2)–Rh(1)–S(2)	110.83(5)	103.80(5)	110.92(3)	112.02(4)
P(1)–Rh(1)–B(3)	112.65(17)	112.83(19)	114.79(11)	116.40(12)
P(2)–Rh(1)–B(3)	112.42(16)	112.3(2)	108.42(11)	104.50(13)
B(3)–Rh(1)–S(2)	119.02(16)	119.79(18)	120.32(11)	121.22(12)

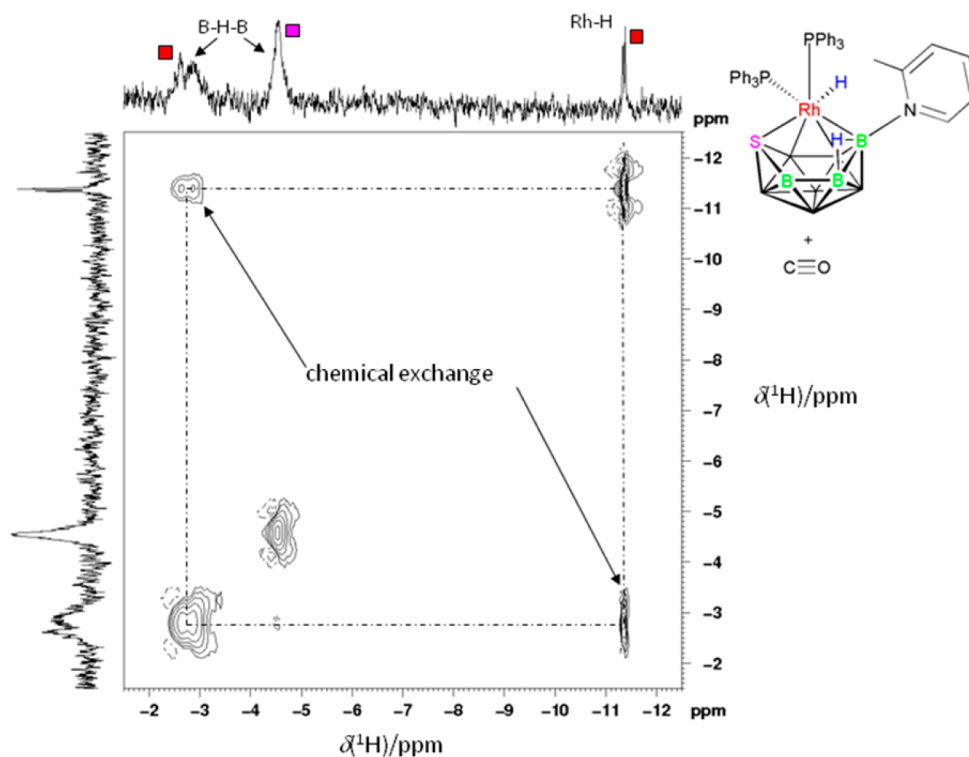


Figure 5. [¹H–¹H]-NOESY at 273 K in CD₂Cl₂ of the reaction mixture formed after the treatment of 3 with CO. The off-diagonal peaks are of the same phase as the diagonal peaks, indicating chemical exchange.

insights dealing with the mechanism of hydrogen loss from these clusters. These results are, therefore, relevant to the reverse reaction: the addition of H₂ to some 11-vertex *isonido*-rhodathiaboranes.^{6a,7} The following paragraphs describe these results.

Carbon monoxide was bubbled for 2 min through a CD₂Cl₂ solution of the 2-picoline ligated hydridorhodathiaborane 3 in a 5 mm NMR tube at room temperature, and the resulting

reaction mixture was then studied by variable-temperature (VT) multi-element NMR spectroscopy, starting at low temperatures. At –50 °C, the ³¹P{¹H} spectrum shows a sharp doublet at δ_p +35.0 ppm and a very broad peak at δ_p +33.8 ppm, together with free PPh₃ and small amounts of O=PPh₃. Interestingly, at 0 °C, the broad signal sharpens and shifts toward higher frequency to become a doublet that overlaps the highest intensity doublet (Figure S2 (Supporting Informa-

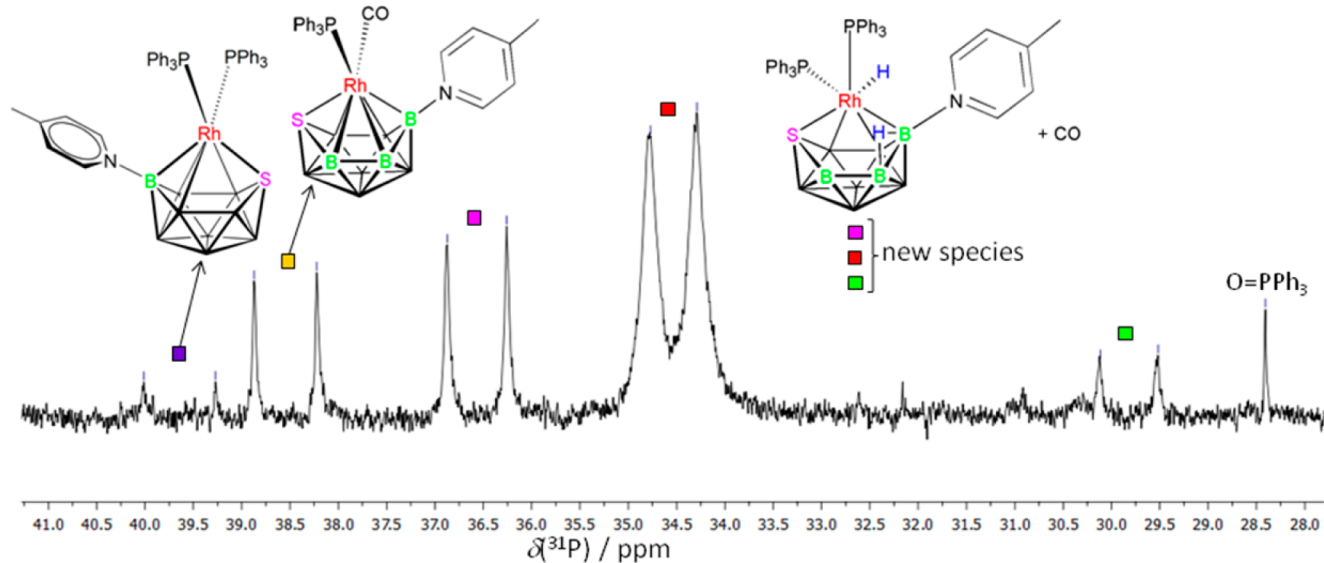


Figure 6. $^{31}\text{P}\{^1\text{H}\}$ NMR spectrum in CD_2Cl_2 of compound **5** after treatment with CO at 223 K.

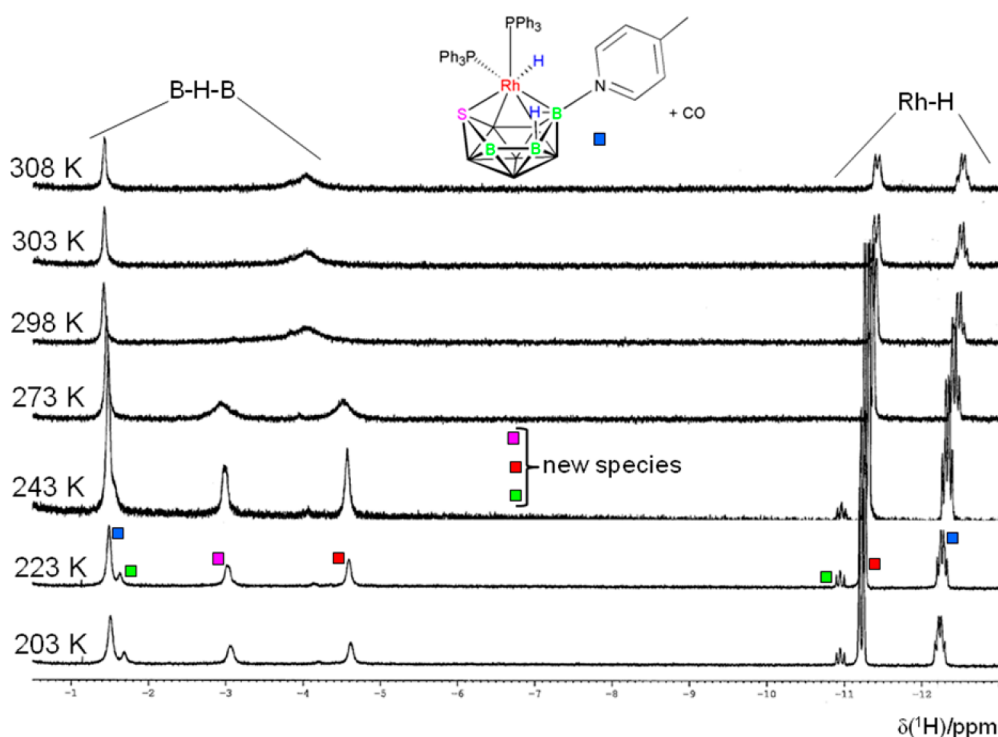


Figure 7. VT $^1\text{H}\{^{11}\text{B}\}$ NMR spectra at different temperatures of **5** after treatment with CO. The peaks labeled with blue squares correspond to the starting reactant **5**.

tion)). The $^1\text{H}\{^{11}\text{B}\}$ NMR spectra at -70 and -50 °C show three peaks in the negative region. The two broad signals at $\delta_{\text{H}} -2.93$ and -4.67 ppm can be assigned to B–H–B bridging hydrogen atoms, which typically occupy positions at B–B edges on the nontriangulated open faces of boron-based clusters. The sharp doublet at $\delta_{\text{H}} -11.33$ ppm corresponds to a Rh–H hydride ligand. The ^1H NMR hydride resonance broadens considerably as the temperature rises, indicating that the hydride ligand is undergoing site exchange (Figure S3 (Supporting Information)). This is confirmed by a $[\text{H}^1\text{H}]$ -NOESY experiment at 0 °C that shows off-diagonal peaks of the same phase as the diagonal peak between the broad B–H–

B proton signal at -2.93 ppm and the Rh–H hydride resonance (Figure 5).

Similarly, the reaction mixtures resulting from the bubbling of CO for several minutes through CD_2Cl_2 solutions of the hydridorhathaboranes **2**, **4**, and **5**, at room temperature, were studied by VT NMR spectroscopy starting at low temperature. For the three systems, the $^{31}\text{P}\{^1\text{H}\}$ NMR spectra at -50 °C exhibit three doublets at around $+36.5$, $+34.5$, and $+29.2$ ppm. In the three samples studied, the highest intensity signal corresponds to the peak close to $+34$ ppm, whereas the doublet at highest field exhibits the lowest intensity (Figure 6). The $^{31}\text{P}\{^1\text{H}\}$ spectra showed free PPh_3 and OPPh_3 , together

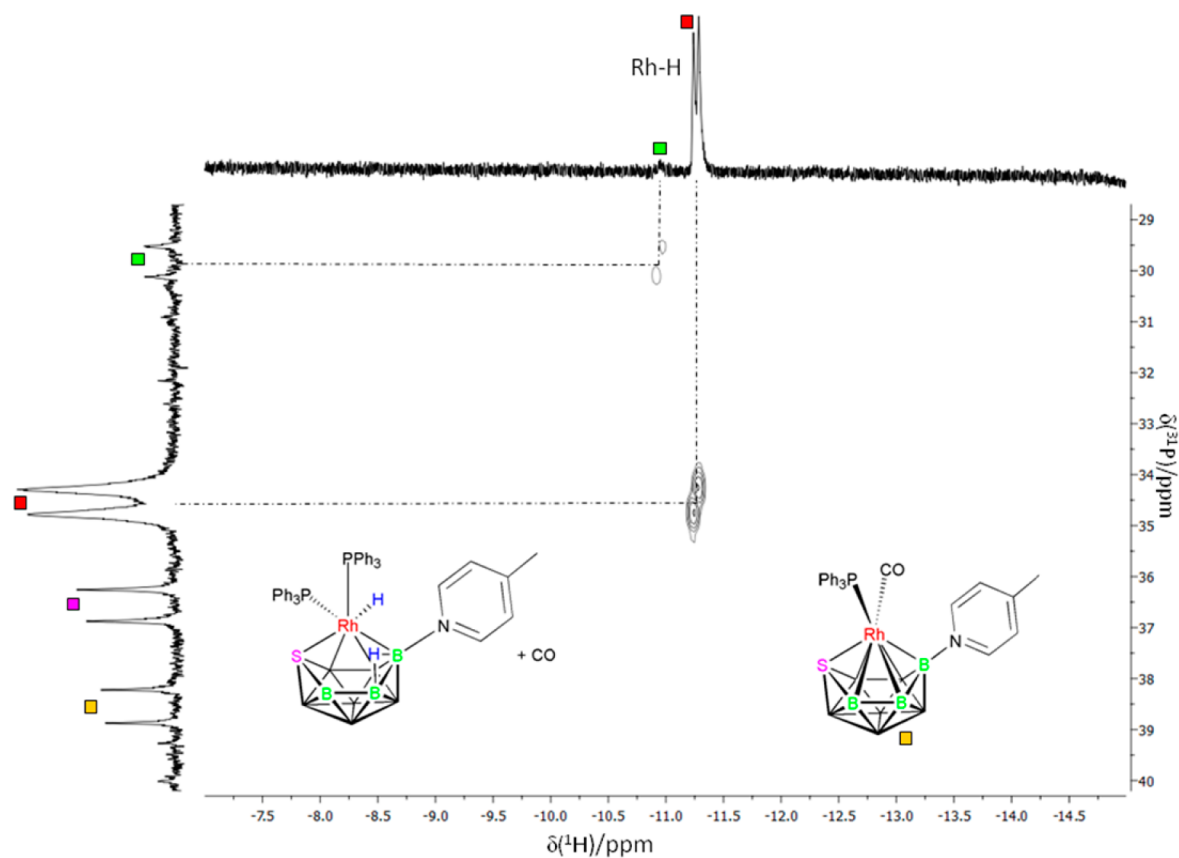


Figure 8. $[^{31}\text{P}-^1\text{H}]$ -HMBC experiment at 223 K of **5** after treatment with CO.

with different amounts of the products of H_2 loss **8**, **10**, and **11** and the products of H_2 loss and CO binding **16**, **18**, and **19**.

Interestingly, at higher temperatures these $^{31}\text{P}\{^1\text{H}\}$ resonances (purple, red, and green squares in Figure 6 and Figures S7–S10 (Supporting Information)) broaden and shift, suggesting that the species are undergoing processes of interconversion in solution.

The $^1\text{H}\{^{11}\text{B}\}$ NMR spectra of the pyridine and 3- and 4-picoline ligated systems with CO each show two broad singlets at δ_{H} ca. -3.0 and -4.5 ppm and a sharp doublet at ca. -11.5 ppm (Figure 7). This pattern resembles the $^1\text{H}\{^{11}\text{B}\}$ spectra discussed above for the 2-picoline system (Figure S3 (Supporting Information)), and, following the same rationale, the broad resonances can therefore be assigned to B–H–B bridging hydrogen atoms and the low-frequency doublet to a Rh–H hydride ligand.

It should be noted that, in the $^1\text{H}\{^{11}\text{B}\}$ spectra of the pyridine and 3- and 4-picoline ligated species, there are two new low-intensity peaks: one at around δ_{H} -1.7 ppm and the other at around -11.0 ppm (green squares in Figures 7 and 8 and Figures S5 and S6 (Supporting Information)). These signals may be attributed to a B–H–B bridging hydrogen atom and a hydride ligand of a new isomer that is not observed in the reaction with the 2-picoline ligated derivative **3**.

For the three systems formed upon treatment of **2**, **4**, and **5** with CO, the small-intensity peaks (green squares) disappear as the temperature increases, whereas the two resonances at around δ_{H} -3.0 and -4.5 ppm broaden and coalesce into a broad peak (Figure 7). This VT NMR behavior clearly contrasts with that of the 2-picoline derivative described earlier where, as the temperature increases, the rearrangement process

involves the hydride ligand and one of the B–H–B hydrogen atoms (Figure 5 and Figure S3 (Supporting Information)).

For the 2-picoline system, a $[^{31}\text{P}-^1\text{H}]$ -HMBC experiment at 223 K showed a correlation between the broad ^{31}P doublet of lower intensity and the hydride resonance (Figure S4 (Supporting Information)). Similarly, the mixtures formed from the reactions of **2**, **4**, and **5** with CO exhibited $[^{31}\text{P}-^1\text{H}]$ -HMBC spectra with correlations between the highest intensity ^{31}P and ^1H doublets and between the lowest intensity ^{31}P and ^1H signals (Figure 8).

Stereochemical Nonrigidity. The observations described above permit us to conclude that the reactions with CO lead to the formation of the substitution products $[8,8,8-(\text{CO})(\text{H})-(\text{PPh}_3)_9-(\text{L})\text{-}n\text{-ido-}8,7\text{-RhSB}_9\text{H}_9]$, where $\text{L} = \text{NC}_5\text{H}_5$, 2-Me- NC_5H_4 , 3-Me- NC_5H_4 , 4-Me- NC_5H_4 , which, according to the $^1\text{H}\{^{11}\text{B}\}$ and $^{11}\text{B}\{^1\text{H}\}$ NMR data (Figures S12 and S13 (Supporting Information)), maintain the 11-vertex *nido* cage of their bis- PPh_3 ligated precursors **2**–**5**.

The data demonstrate the formation of two new species in the 2-picoline reaction system upon treatment with CO, whereas for the pyridine and 3- and 4-picoline containing clusters, there are clearly three new compounds. These species are stable at low temperatures, but at room and higher temperatures they undergo hydrogen loss and a consequent *nido* to *closo* (or *isonido*) cluster structural transformation. The VT NMR data show that the intermediates interconvert. More specifically, it may be proposed that these labile rhodathiaboranes are isomers that exhibit different $\{\text{Rh}(\text{CO})(\text{H})(\text{PPh}_3)\}$ to $\{\eta^4\text{-SB}_9\text{H}_9(\text{L})\}$ configurations ($\text{L} = \text{pyridine}$, 2-, 3-, or 4-picoline). In other words, the substitution of a PPh_3 ligand by

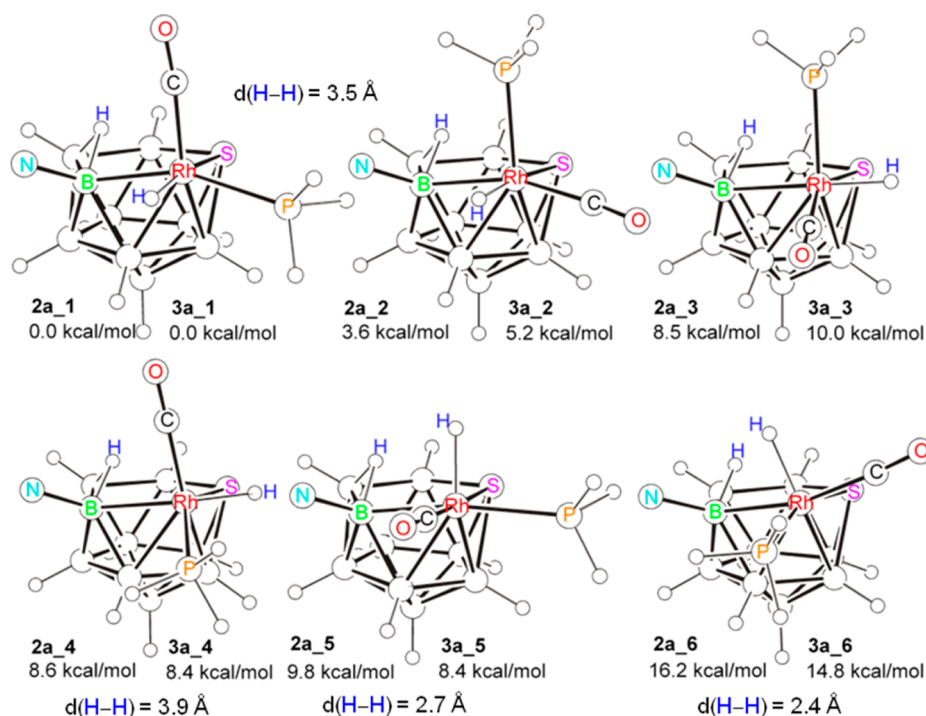


Figure 9. Energy comparisons for DFT optimized metal to thiaborane configurational isomers of the pyridine ligated model **2a** and of the 2-picoline ligated counterpart **3a**.

CO appears to enhance the stereochemical nonrigidity of the metal–thiaborane linkage, favoring isomerization processes.

The NMR data show that two of the three isomers detected in the reactions of CO with **2**, **4**, and **5** are very similar to the two species detected in the system with the 2-picoline counterpart **3** (Figure S3 (Supporting Information) and Figure 7). However, the interconversions between the species appear to be different.

A priori, these findings may be rationalized in terms of the different steric requirements of the 2-picoline substituent in comparison to pyridine, 3-picoline, and 4-picoline, resulting in different energy barriers for the transition states of the structural rearrangement processes together with stabilization of the products.

DFT Study. In order to attain more insight into the fluxional and exchange processes involved in the compounds reported here, we carried out density functional theory (DFT) calculations on model structures. The PPh₃ ligands were replaced by PH₃ to reduce calculation time.

Thus, DFT calculations on [8,8,8-(CO)(H)(PH₃)-9-(NC₅H₅)-nido-8,7-RhSB₉H₉] (**2a**) and [8,8,8-(CO)(H)(PH₃)-9-(2-Me-NC₅H₄)-nido-8,7-RhSB₉H₉] (**3a**) demonstrate that, of the six possible spatial combinations of the ligands around the metal center, the most stable is that in which the hydride lies trans to the sulfur vertex, the CO ligand lies trans to the B(3)–B(4) edge, and the PH₃ group occupies a position trans to the B(9) vertex (Figure 9). The pyridine and 2-picoline isomers **2a**₁–**2a**₆ and **3a**₁–**3a**₆ follow the same relative energy trend.

It is interesting to note that, for the 2-picoline ligated isomers, the conformers in which the methyl group is adjacent to the pentagonal open face of the cluster are more stable than those in which this substituent is oriented toward the B(1) vertex. In some of the 2-picoline ligated isomers, a conformational change around the N–B(9) bond has an energy penalty

as large as 5.5 kcal/mol (see Figure S14 (Supporting Information)).

It has been previously demonstrated that substitution reactions of **2** with monodentate phosphines follow dissociative mechanisms, the dissociation of the PPh₃ ligand trans to the B(9) vertex being more favored.⁹ It is reasonable to expect, therefore, that the treatment of **2** and **3** with CO under the conditions described above (short reaction times and low temperatures) is more likely to result in the substitution of the PPh₃ trans to the B(9) vertex. Under this assumption, the PH₃ models **2a**₂ and **3a**₂ would correspond to the kinetic reaction products, whereas the isomers **2a**₁ and **3a**₁ would be the thermodynamic products (Figure 9).

Following this analysis, we can conclude that the major intermediate (red square signals in Figures 5–8) is more likely to be the isomer with a metal to thiaborane configuration which resembles that in **2a**₂ and **3a**₂ (Figure 9). A pseudorotation of the {Rh(H)(CO)(PPh₃)} group relative to the η⁴-{SB₉H₉(L)} moiety can afford different metal to thiaborane configurations that can account for the intermediates that are observed by NMR at low temperatures.

A clockwise {Rh(H)(CO)(PH₃)} to η⁴-{SB₉H₉(L)} rotation in the isomers **2a**₁, **2a**₂, **3a**₁, and **3a**₂ results in the formation of the corresponding isomers, **2a**₆, **2a**₅, **3a**₆, and **3a**₅. These intermediates (Rh–H hydride trans to boron vertices) exhibit higher energies than the parent isomers (Rh–H hydride trans to S(7)). However, this type of metal–thiaborane pseudorotation draws the B(9)–B(10) bridging hydrogen atom closer to the hydride ligand, facilitating its chemical exchange. Thus, intermediates **3a**₅ and **3a**₆ can account for the VT NMR behavior observed in the 2-picoline system (Figure 5 and Figure S3 (Supporting Information)).

Regarding the second major intermediate (purple squares in Figures 5–8), this species does not feature a Rh–H hydride ligand and therefore the DFT-calculated isomers depicted in

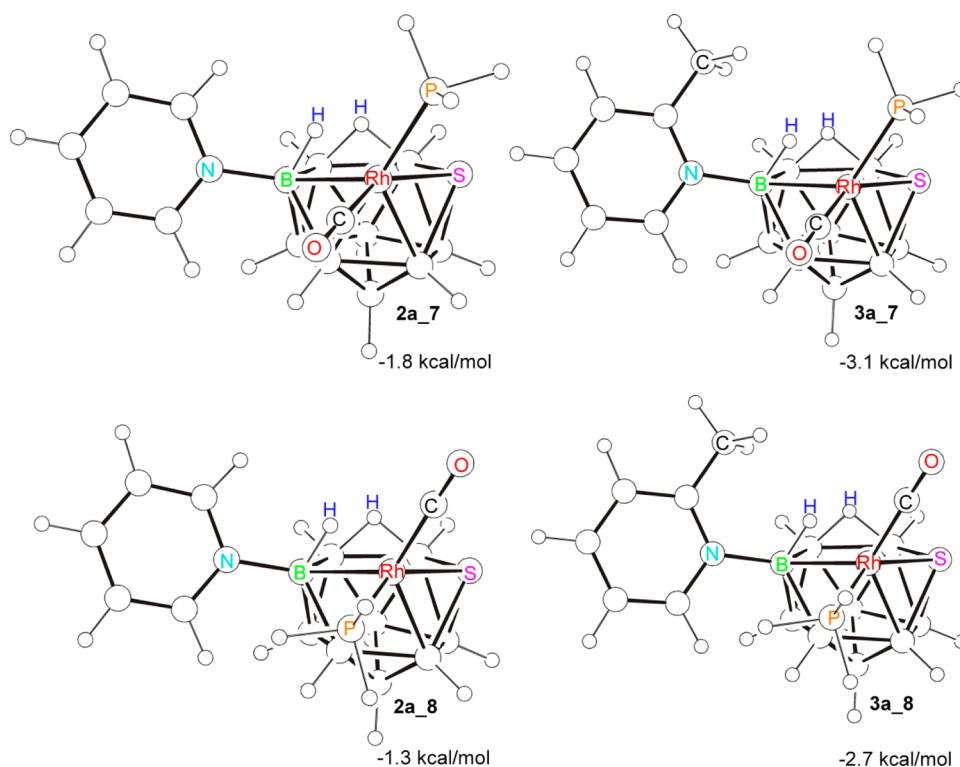


Figure 10. DFT-calculated rotational isomers for the PH_3 ligated models **2a** and **3a** with two hydrogen atoms on the pentagonal open face along the B(10)–B(11) and B(9)–Rh(8) edges.

Scheme 6. Proposed Tautomerization Processes in CO-Ligated Rhodathiaboranes Preceding H_2 Loss

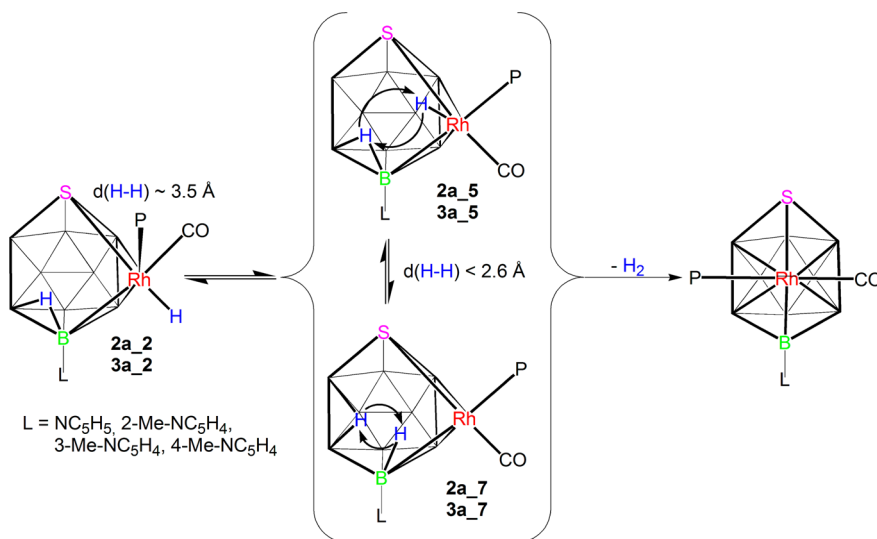


Figure 9 do not provide reasonable models that could account for the structure of this second derivative. Consequently, in the search for other plausible intermediates, we carried out DFT calculations using as starting points isomers with bridging hydrogen atoms along the Rh(8)–B(9) and B(10)–B(11) edges of the pentagonal face. The optimizations gave the isomers **2a_7**, **2a_8**, **3a_7**, and **3a_8**, of lower energy than the hydride ligated clusters (Figures 9 and 10). In these calculated PH_3 models, one hydrogen atom occupies a position along the Rh(8)–B(9) edge in a clearly asymmetric fashion almost 2.0 Å from the metal center, whereas the other hydrogen atom bridges the B(10)–B(11) edge (Figure 10). In this new configuration, these two hydrogen atoms are 2.06 Å apart, this

allowing a facile chemical exchange between the two nuclear positions on the pentagonal open face. This fluxional process would lead to a single proton resonance in the negative region of the $^1\text{H}\{^{11}\text{B}\}$ NMR spectra. Following this discussion, it is reasonable to propose that the second major isomer is a cluster that exhibits a nuclear configuration similar to that of the models **2a_7**, **2a_8**, **3a_7**, and **3a_8** and that the two hydrogen atoms on the pentagonal face undergo fast exchange at both low and high temperatures, rendering both protons indistinguishable on the NMR time scale (purple squares in Figures 5–8). Related to this process is, for example, the low-energy barrier tautomerism of the endo/bridging H atoms in $[\text{B}_{11}\text{H}_{14}]^{-21}$.

In view of these DFT results, it may be proposed that the hydride ligated isomers found in the pyridine and 3- and 4-picoline systems, model **2a₂**, interconvert with the second major isomers, model **2a₇**, at higher temperatures (Scheme 6). Under the same conditions, the 2-picoline ligated analogues do not undergo significant interconversion. However, as indicated above, the hydride ligated species, represented by **3a₂**, undergo intramolecular exchange between the Rh–H hydride ligand and the B–H–B bridging hydrogen atom, most probably through metal–thiaborane pseudorotations that bring the two hydrogen atoms closer, as suggested in the isomer **3a₅**.

The different behavior in the interconversion of the CO ligated pyridine and 3- and 4-picoline isomers versus the CO ligated 2-picoline counterparts suggests that the rearrangement processes involved in the proposed **2a₂** ↔ **2a₅** ↔ **2a₇** tautomerizations (Scheme 6) have lower energy barriers for the pyridine and 3- and 4-picoline ligated clusters than for the 2-picoline analogues. However, the exchange of the hydride ligand and the B–H–B bridging hydrogen atom, which should involve cluster rearrangements of the type **2a₂** ↔ **2a₅** and **3a₂** ↔ **3a₅**, is favored in the 2-picoline ligated isomers, probably because the energy barrier between the hydride species **3a₅** and the other isomer **3a₇** is higher than that in the pyridine and 3- and 4-picoline derivatives (Scheme 6).

It should be noted that a related mechanism of hydrogen M–H/B–H–M exchange, involving key M–(η^2 -H₂) intermediates, has been reported for *exo-nido*-osmacarboranes that exhibit {Os(H)₂(PPh₃)₂} fragments exopolyhedrically linked to 11-vertex *nido*-carborane ligands, [7-R-7,9-C₂B₉H₉]²⁻, via two B–H–Os bonds.²²

It is worth mentioning that the {Rh(H)(CO)(L)} to η^4 -{SB₉H₉(L)} pseudorotations described earlier are related to the well-known rotational twisting of exopolyhedral metal-containing fragments bound through (BH)_n–M interactions to *nido*-carboranes.²³ In addition, the flexibility of heteroboranes as face-bound ligands is well documented in, for example, metallacarboranes and metallathiaboranes.²⁴ In the case of 11-vertex rhodathiaboranes, the parent cluster **1** undergoes an interesting fluxional process that involves a hindered rotation with respect to the {SB₉H₁₀} fragment.⁴ Recently, we have proved that the introduction of carbenes as exopolyhedral ligands or protonation of the clusters results in an enhancement of the nonrigidity in the metal-to-thiaborane linkage, opening new ways of fluxional and exchange processes.^{7,8,11} The CO ligand appears to induce an analogous lability in the metal–thiaborane connection.

CONCLUSIONS

It has been shown that the previously reported reaction between the rhodathiaborane [8,8-(PPh₃)₂-*nido*-8,7-RhSB₉H₁₀] (**1**) and pyridine to give the hydridorhodathiaborane [8,8,8-(H)(PPh₃)₂-9-(NC₅H₅)-*nido*-8,7-RhSB₉H₉] (**2**) can be extended to the 2-, 3-, and 4-methylpyridine isomers, affording in good yields the corresponding picoline ligated hydridorhodathiaboranes **3–5**. These results illustrate the scope of this reaction that, in principle, can be carried out with a vast number of N-heterocyclic ligands.

The 3- and 4-picoline ligated hydrides (**4** and **5**) exhibit a thermal stability toward dehydrogenation and *nido-closo* structural transformation that is similar to that of the pyridine counterpart **2**. However, the 2-picoline analogue loses hydrogen significantly faster.

The reactions of picoline ligated hydridorhodathiaboranes **3–5** with C₂H₄ and CO in this report resemble those found for the pyridine analogue **2**, giving products of ligand substitution and cluster dehydrogenation **12–19**. These reactions nicely illustrate the structural flexibility and chemical tunability of these 11-vertex clusters and demonstrate that the parent rhodathiaborane [8,8-(PPh₃)₂-*nido*-8,7-RhSB₉H₁₀] (**1**), first reported in 1990,⁴ is actually a rich source of organometallic chemistry.

The study of the reactions between the hydridorhodathiaboranes and CO at low temperatures has allowed the identification of intermediates that have provided new insights into the loss of hydrogen from the clusters. Upon the substitution of one of the PPh₃ ligands by CO, the clusters become more reactive, undergoing, at low temperature, intramolecular as well as intermolecular exchange processes that are a consequence of the increased cluster nonrigidity. The dynamic behavior observed for the 2-picoline system is different to that of the pyridine and 3- and 4-picoline systems, with DFT calculations supporting the proposition that the difference in cluster fluxionality may be attributed to the steric effect of the methyl group of the 2-methyl-pyridine substituent. The intramolecular exchange between the hydride ligand and the B–H–B bridging hydrogen atom found at low temperatures for the 2-picoline system is also relevant here because it should involve a transition state in which the two hydrogen atoms reach a close proximity in the cluster, representing therefore a crucial step toward hydrogen loss. Although the detailed mechanism is unclear, the formation of Rh–(η^2 -H₂) intermediates could facilitate the exchange of the hydrogen atoms at low temperatures. In this regard, we have recently reported that dihydrogen activation on a carbene ligated rhodathiaborane takes place through structural transformations of the cluster, involving the formation of dihydrogen ligated intermediates.⁷ For the carbonyl intermediates, the final release could occur similarly via H₂ coordination to the rhodium center.

EXPERIMENTAL SECTION

General Considerations. All reactions were carried out under an argon atmosphere using standard Schlenk-line techniques. Solvents were obtained from an Innovative Technology Solvent Purification System. All commercial reagents were used as received without further purification. The rhodathiaborane [8,8-(PPh₃)₂-*nido*-8,7-RhSB₉H₁₀] (**1**) was prepared by published methods.⁴

¹H and ¹¹B NMR data, focused on cluster B–H units, are gathered in Tables 3–5. Additional ¹H NMR data are given below.

NMR spectra were recorded on Bruker Avance 300 MHz, AV 400 MHz, and AV 500 MHz spectrometers, using ¹¹B, ¹¹B{¹H}, ¹H, ¹H{¹¹B}, ¹H{¹¹B(selective)},²⁵ ³¹P{¹H}, [¹H–¹H]-NOESY, and [¹H–³¹P]-HMBC techniques.²⁶ ¹H chemical shifts were measured relative to partially deuterated solvent peaks but are reported in ppm relative to tetramethylsilane. ¹¹B chemical shifts were measured relative to BF₃·OEt₂. ³¹P chemical shifts were measured relative to H₃PO₄ (85%). Mass spectrometry data were recorded on a VG Autospec double-focusing mass spectrometer, on a Microflex MALDI-TOF instrument, and on a ESQUIRE 3000+ API-TRAP instrument, operating in either positive or negative mode. In each case there was an excellent correspondence between the calculated and measured isotopomer envelopes. A well-matched isotope pattern may be taken as a good criterion of identity.²⁷

GC analyses were performed on either a Hewlett-Packard HP 5890 Series II gas chromatograph equipped with a flame ionization detector and a 25 m (0.32 mm inner diameter, 0.17 mm film thickness) HP-Ultra-1 column or on an Agilent 6890 Series GC system equipped

with an Agilent 5973 mass-selective detector and a 30 m (0.25 mm i.d., 0.25 mm f.t.) HP-SMS column.

X-ray Structure Analysis of Crystals of 4, 5, and 9. Crystals were grown by slow diffusion of hexane into dichloromethane solutions. In all cases, the crystals were coated with perfluoropolyether, mounted on a glass fiber, and fixed in a cold nitrogen stream ($T = 100(2)$ K) to the goniometer head. Data collections were performed on a Bruker Kappa APEX DUO CCD area detector diffractometer with monochromatic radiation ($\lambda(\text{Mo } K\alpha) = 0.7107073 \text{ \AA}$, using narrow frames (0.3° in ω). The data were reduced (SAINT)²⁸ and corrected for absorption effects by multiscan methods (SADABS).²⁹ The structure was solved using the SHELXS-86 program³⁰ and refined against all F^2 data by full-matrix least-squares techniques (SHELXL-97).³¹ All non-hydrogen atoms were refined with anisotropic displacement parameters. Hydrogen atoms were included in calculated positions and refined with a positional and thermal riding model.

Calculations. All DFT calculations were performed using the Gaussian 09 package.³² Structures were initially optimized using standard methods with the STO-3G* basis-sets for C, B, P, S, and H with the LANL2DZ basis set for the rhodium atom. The final optimizations, including frequency analyses to confirm the true minima, were performed using B3LYP methodology, with the 6-31G* and LANL2DZ basis sets. The GIAO nuclear shielding calculations were performed on the final optimized geometries, and computed ^{11}B shielding values were related to chemical shifts by comparison with the computed value for B_2H_6 , which was taken to be $\delta(^{11}\text{B}) + 16.6$ ppm relative to the $\text{BF}_3 \cdot \text{OEt}_2$ 0.0 ppm standard.

Synthesis of Picoline-Ligated 11-Vertex Hydridorhodathiorboranes 3–5. *[8,8,8-H(PPH₃)₂-9-(2-Me-NC₅H₄)-nido-8,7-RhSB₉H₉]* (**3**). In a Schlenk tube, 100 mg (0.130 mmol) of **1** was dissolved in 10 mL of CH_2Cl_2 , resulting in a bright red solution. A 190 μL portion (182 mg, 1.95 mmol) of 2-methylpyridine was syringed into the solution, and the reaction mixture was stirred at room temperature for 4 h to give a 1:1 mixture of **3** and its dehydrogenation product $[1,1-(\text{PPh}_3)_2-3-(2\text{-Me-Py})\text{-}closo\text{-}1,2\text{-RhSB}_9\text{H}_8]$. This mixture was cooled to liquid nitrogen temperature, and the vessel was evacuated and then exposed to a hydrogen-filled balloon. The resulting system was stirred at room temperature for 4 h. After this time, the solvent was evaporated to dryness and the residue washed three times with $\text{CH}_2\text{Cl}_2/\text{hexane}$, to obtain **3**. Yield: 97.0 mg, 0.112 mmol, 87%. Anal. Calcd for $\text{C}_{42}\text{H}_{47}\text{B}_9\text{NP}_2\text{RhS}$: C, 58.65; H, 5.51; N, 1.63; S, 3.73. Found: C, 58.23; H, 5.41; N, 1.25; S, 3.98. IR (ATR, cm^{-1}): ν 2502 vs (BH), 2042 m (RhH). ^1H NMR (300 MHz, CD_2Cl_2 , 300 K): δ 8.97 (d, 2H, 2- $\text{CH}_3\text{-NC}_5\text{H}_4$), 8.02 (m, 1H, 2- $\text{CH}_3\text{-NC}_5\text{H}_4$), 7.69 (m, 1H, 2- $\text{CH}_3\text{-Py}$), 7.23–7.00 (30H, 2 PPh_3), 3.10 (s, 3H, 2- $\text{CH}_3\text{-Py}$). $^{31}\text{P}\{^1\text{H}\}$ NMR (121 MHz, CD_2Cl_2 , 300 K): δ +34.5 [br dd, $^1J_{\text{RhP}} = 97.66$ Hz, $^2J_{\text{PP}}$ not resolved due to the broadness of the peak], +32.6 [dd, $^1J_{\text{RhP}} = 129$ Hz, $^2J_{\text{PP}} = 18.3$ Hz]. $^{31}\text{P}\{^1\text{H}\}$ NMR (121 MHz, CD_2Cl_2 , 243 K): δ +36.6 [br dd, $^1J_{\text{RhP}} = 106$ Hz, $^2J_{\text{PP}}$ not resolved due to the broadness of the peak], +32.3 [dd, $^1J_{\text{RhP}} = 125$ Hz, $^2J_{\text{PP}} = 19$ Hz]. LRMS (MALDI⁺): m/z 596 $[\text{M} - (\text{PPh}_3) - 2\text{H}]^+$. Isotope envelopes match those calculated from the known isotopic abundances of the constituent elements.

[8,8,8-H(PPH₃)₂-9-(3-Me-NC₅H₄)-nido-8,7-RhSB₉H₉] (**4**). To a bright yellow solution of 100 mg (0.131 mmol) of **1** in 10 mL of CH_2Cl_2 was added 127 μL (121 mg; 1.30 mmol) of 3-methylpyridine. After 4 h of stirring at room temperature under an atmosphere of argon, the solvent was evaporated to dryness and the solid residue washed three times with hexane. The final product was characterized as compound **4**. Yield: 91.0 mg, 0.106 mmol, 81%. Anal. Calcd for $\text{C}_{42}\text{H}_{47}\text{B}_9\text{NP}_2\text{RhS} \cdot 2\text{CH}_2\text{Cl}_2$: C, 51.31; H, 4.99; N, 1.36; S, 3.11. Found: C, 50.82; H, 5.03; N, 1.31; S, 2.35. IR (ATR, cm^{-1}): ν 2529 vs (BH), 2040 m (RhH). ^1H NMR (300 MHz, CD_2Cl_2 , 300 K): δ 7.96 (m, 2H; 3- $\text{CH}_3\text{-NC}_5\text{H}_4$), 7.68 (m, 1H; 3- $\text{CH}_3\text{-NC}_5\text{H}_4$), 7.33 (t, 1H; 3- $\text{CH}_3\text{-NC}_5\text{H}_4$), 7.31–7.04 (30H, 2 PPh_3), 2.20 (s, 3H, 3- $\text{CH}_3\text{-NC}_5\text{H}_4$). $^{31}\text{P}\{^1\text{H}\}$ NMR (121 MHz, CD_2Cl_2 , 300 K): δ +32.7 [d, $^1J_{\text{RhP}} = 120$ Hz; 2 PPh_3]. $^{31}\text{P}\{^1\text{H}\}$ NMR (121 MHz, CD_2Cl_2 , 243 K) δ +35.7 [br dd, $^1J_{\text{RhP}} = 103$ Hz; $^2J_{\text{PP}}$ not resolved due to the broadness of the peak], +30.7 [dd, $^1J_{\text{RhP}} = 128$ Hz; $^2J_{\text{PP}} = 19$ Hz]. LRMS (MALDI⁺): m/z 596

$[\text{M} - (\text{PPh}_3) - 2\text{H}]^+$. Isotope envelopes match those calculated from the known isotopic abundances of the constituent elements.

[8,8,8-H(PPH₃)₂-9-(4-Me-NC₅H₄)-nido-8,7-RhSB₉H₉] (**5**). In a Schlenk tube, a solution of **1** (300 mg, 0.393 mmol) in 15 mL of CH_2Cl_2 was treated with 381 μL (363 mg; 3.90 mmol) of 4-methylpyridine. The reaction mixture was stirred at room temperature under an atmosphere of argon for 4 h, the solvent was evaporated to dryness, and the residue was washed three times with hexane to isolate **5**. Yield: 255 mg, 0.296 mmol, 75%. Anal. Calcd for $\text{C}_{42}\text{H}_{47}\text{B}_9\text{NP}_2\text{RhS} \cdot \text{CH}_2\text{Cl}_2$: C, 54.65; H, 5.23; N, 1.48; S, 3.39. Found: C, 54.18; H, 5.48; N, 1.46; S, 3.41. IR (ATR, cm^{-1}): ν 2520 vs (BH), 2465 vs (BH), 2033 m (RhH). ^1H NMR (300 MHz, CD_2Cl_2 , 300 K): δ 7.70 (d, 2H; 4- $\text{CH}_3\text{-NC}_5\text{H}_4$), 7.36 (t, 2H; 4- $\text{CH}_3\text{-NC}_5\text{H}_4$), 7.26–6.85 (30H, 2 PPh_3), 2.27 (m, 3H, 4- $\text{CH}_3\text{-NC}_5\text{H}_4$). $^{31}\text{P}\{^1\text{H}\}$ NMR (121 MHz, CD_2Cl_2 , 300 K): δ 33.0 [d, $^1J_{\text{RhP}} = 121$ Hz; 2 PPh_3]. $^{31}\text{P}\{^1\text{H}\}$ NMR (121 MHz, CD_2Cl_2 , 203 K) δ 37.0 [br dd, $^1J_{\text{RhP}} = 107$ Hz; $^2J_{\text{PP}}$ not resolved due to the broadness of the peak], 30.0 [dd, $^1J_{\text{RhP}} = 128$ Hz; $^2J_{\text{PP}} = 18$ Hz]. LRMS (MALDI⁺): m/z 596 $[\text{M} - (\text{PPh}_3) - 2\text{H}]^+$. Isotope envelopes match those calculated from the known isotopic abundances of the constituent elements.

Preparation of Bis-PPh₃-Ligated *closo*-Rhodathiorboranes 9–11. As a general procedure, a 10-fold excess of PPh_3 was added to a solution of the corresponding ethylene ligated rhodathiorboranes **13–15**, which were dissolved in 10 mL of CH_2Cl_2 . The orange-red solution was stirred at room temperature for several hours to give a red solution. The solvent was evaporated to dryness and the residue washed three times with hexane. The final solids were recrystallized from $\text{CH}_2\text{Cl}_2/\text{hexane}$ to give the bis- PPh_3 ligated rhodathiorboranes $[1,1-(\text{PPh}_3)_2-3(\text{L})\text{-}closo\text{-}1,2\text{-RhSB}_9\text{H}_8]$, where L = 2-Me-NC₅H₄ (**9**), 3-Me-NC₅H₄ (**10**), 4-Me-NC₅H₄ (**11**).

[1,1-(PPH₃)₂-3-(2-Me-NC₅H₄)-closo-1,2-RhSB₉H₈] (**9**). The reaction was carried out with 120 mg (0.458 mmol) of PPh_3 and 30 mg (0.048 mmol) of $[1,1-(\text{PPh}_3)(\eta^2\text{-C}_2\text{H}_4)\text{-}3\text{-}(2\text{-Me-NC}_5\text{H}_4)\text{-}closo\text{-}1,2\text{-RhSB}_9\text{H}_8]$ (**13**), with stirring for 6 h. Yield: 35 mg, 0.0408 mmol, 85%. Anal. Calcd for $\text{C}_{42}\text{H}_{45}\text{B}_9\text{NP}_2\text{RhS} \cdot \text{CH}_2\text{Cl}_2$: C, 54.77; H, 5.02; N, 1.49; S, 3.40. Found: C, 54.42; H, 4.91; N, 1.17; S, 3.44%. IR (ATR, cm^{-1}): ν 2568 vs (BH), 2492 vs (BH), 2456 vs (BH), 1259 m (BH), 1079 s, 1001 s, 797 m, 690 vs ^1H NMR (300 MHz, CD_2Cl_2 , 300 K): δ 8.89 (d, 2H, 2- $\text{CH}_3\text{-NC}_5\text{H}_4$), 8.07 (m, 1H, 2- $\text{CH}_3\text{-NC}_5\text{H}_4$), 7.72 (m, 2H, 2- $\text{CH}_3\text{-NC}_5\text{H}_4$), 7.50–7.00 (30H, 2 PPh_3), 3.04 (s, 3H, 2- $\text{CH}_3\text{-NC}_5\text{H}_4$). $^{31}\text{P}\{^1\text{H}\}$ NMR (161 Hz, CD_2Cl_2 , 183 K): +41.4 (1P, dd, $^1J_{\text{P-Rh}} = 145$ Hz, $^2J_{\text{P-P}} = 22$), +34.3 (1P, dd, $^1J_{\text{P-Rh}} = 152$). $^{31}\text{P}\{^1\text{H}\}$ NMR (121 MHz, CD_2Cl_2 , 300 K): δ +38.7 [d, $^1J_{\text{RhP}} = 149$ Hz; 2 PPh_3]. LRMS (MALDI⁺/DCTB): m/z 596 $[\text{M} - (\text{PPh}_3)]^+$. Isotope envelopes match those calculated from the known isotopic abundances of the constituent elements.

[1,1-(PPH₃)₂-3-(3-Me-NC₅H₄)-closo-1,2-RhSB₉H₈] (**10**). The reaction was carried out with 126 mg (0.480 mmol) of PPh_3 and 30 mg (0.048 mmol) of $[1,1-(\text{PPh}_3)(\eta^2\text{-C}_2\text{H}_4)\text{-}3\text{-}(3\text{-Me-NC}_5\text{H}_4)\text{-}closo\text{-}1,2\text{-RhSB}_9\text{H}_8]$ (**14**), with stirring for 12 h. Yield: 33 mg, 0.0385 mmol, 80%. Anal. Calcd for $\text{C}_{42}\text{H}_{45}\text{B}_9\text{NP}_2\text{RhS} \cdot \text{CH}_2\text{Cl}_2$: C, 54.77; H, 5.02; N, 1.49; S, 3.40. Found: C, 54.33; H, 4.94; N, 1.37; S, 3.34. IR (ATR, cm^{-1}): ν 2569 vs (BH), 2490 vs (BH), 2459 vs (BH), 1258 m (BH), 1081 s, 1003 s, 796 m, 691 vs ^1H NMR (300 MHz, CD_2Cl_2 , 300 K): δ 8.92 (d, 2H, 3- $\text{CH}_3\text{-NC}_5\text{H}_4$), 8.01 (m, 1H, 3- $\text{CH}_3\text{-NC}_5\text{H}_4$), 7.54 (m, 1H, 3- $\text{CH}_3\text{-NC}_5\text{H}_4$), 7.26–7.00 (30H, 2 PPh_3), 2.48 (s, 3H, 3- $\text{CH}_3\text{-NC}_5\text{H}_4$). $^{31}\text{P}\{^1\text{H}\}$ NMR (121 MHz, CD_2Cl_2 , 300 K): δ 40.2 [d, $^1J_{\text{RhP}} = 147$ Hz; 2 PPh_3]. LRMS (MALDI⁺/DCTB): m/z 596 $[\text{M} - (\text{PPh}_3)]^+$. Isotope envelopes match those calculated from the known isotopic abundances of the constituent elements.

[1,1-(PPH₃)₂-3-(4-Me-NC₅H₄)-closo-1,2-RhSB₉H₈] (**11**). The reaction was carried out with 105 mg (0.40 mmol) of PPh_3 and 25 mg (0.040 mmol) of $[1,1-(\text{PPh}_3)(\eta^2\text{-C}_2\text{H}_4)\text{-}3\text{-}(4\text{-Me-NC}_5\text{H}_4)\text{-}closo\text{-}1,2\text{-RhSB}_9\text{H}_8]$ (**15**), with stirring for 16 h. Yield: 26 mg, 0.030 mmol, 75%. Anal. Calcd for $\text{C}_{42}\text{H}_{45}\text{B}_9\text{NP}_2\text{RhS} \cdot 2\text{CH}_2\text{Cl}_2$: C, 51.41; H, 4.80; N, 1.36; S, 3.12%. Found: C, 50.91; H, 4.35; N, 0.88; S, 2.64. IR (ATR, cm^{-1}): ν 2502 vs (BH), 2453 vs (BH), 1264 m (BH), 1085 s, 1004 s, 693 vs ^1H NMR (300 MHz, CD_2Cl_2 , 300 K): δ 8.75 (d, 2H, 4- $\text{CH}_3\text{-NC}_5\text{H}_4$), 7.51 (m, 2H, 4- $\text{CH}_3\text{-NC}_5\text{H}_4$), 7.25–7.03 (30H, 2 PPh_3), 2.73 (s, 3H, 4- $\text{CH}_3\text{-NC}_5\text{H}_4$). $^{31}\text{P}\{^1\text{H}\}$ NMR (121 MHz, CD_2Cl_2 , 300 K): δ

39.6 [d, $^1J_{\text{RHP}} = 153$ Hz; 2PPh₃]. LRMS (MALDI⁺/DCTB): m/z 595 [M - (PPh₃) - H]⁺. Isotope envelopes match those calculated from the known isotopic abundances of the constituent elements.

Synthesis of Ethylene-Ligated *closo*-Rhodathioboranes 13–15. As a general procedure, 100 mg of the corresponding hydridorhodathioborane [8,8,8-(PPh₃)₂H-9-(L)-*nido*-8,7-RhSB₉H₉], where L = 2-Me-NC₅H₄ (3), 3-Me-NC₅H₄ (4), 4-Me-NC₅H₄ (5), was dissolved in 20 mL of CH₂Cl₂ in a Schlenk tube. After three freeze–thaw cycles, a balloon containing ethylene was attached to the Schlenk tube, and the rhodathioborane solution was exposed to the gas. The system was stirred at room temperature. After a variable length of time, the reaction mixture was concentrated by solvent evaporation under vacuum, and hexane was added to produce an orange-red precipitate, which was washed several times with hexane. The solid was crystallized from CH₂Cl₂/hexane to isolate the respective ethylene ligated clusters [1,1-(η²-C₂H₄)(PPh₃)₂-3-(L)-*closo*-1,2-RhSB₉H₉].

[1,1-(PPh₃)₂(η²-C₂H₄)-3-(2-Me-NC₅H₄)-*closo*-1,2-RhSB₉H₉] (13). The reaction was carried out with 100 mg (0.116 mmol) of 3, and the solution was exposed to an ethylene atmosphere for 2 h. Yield: 62 mg, 0.099 mmol, 86%. Anal. Calcd for C₂₆H₃₄B₉NPRhS: C, 50.06; H, 5.49; N, 2.5; S, 5.14. Found: C, 50.26; H, 5.63; N, 2.32; S, 5.01. IR (ATR, cm⁻¹): ν 2528 vs (BH), 2507 vs (BH), 2497 vs (BH), 2472 vs (BH), 2452 vs (BH), 1618 w, 1476 s, 1451 w, 1430 s, 1260 m, 1151 m, 1087 s, 1010 m, 946 m, 748 m, 692 s, 526 s, 492 m, 456 m (Rh-C₂H₄), 418 m (Rh-C₂H₄), 325 w (RhP). ¹H NMR (300 MHz, CD₂Cl₂, 300 K): δ 9.45 (m, 2H, 2-CH₃-NC₅H₅), 8.07 (m, 2H, 2-Me-NC₅H₅), 7.70–7.01 (15H, PPh₃), 3.05 (s, 3H, 2-CH₃-NC₅H₅), 2.16 (m, 2H, C₂H₄), 1.99 (m, 2H, C₂H₄). ³¹P{¹H} NMR (121 MHz, CD₂Cl₂, 300 K): δ 34.19 [d, $^1J_{\text{RHP}} = 134$ Hz, PPh₃]. LRMS (MALDI⁺/DCTB): m/z 595 [M - (C₂H₄) - H]⁺. Isotope envelopes match those calculated from the known isotopic abundances of the constituent elements.

[1,1-(PPh₃)₂(η²-C₂H₄)-3-(3-Me-NC₅H₄)-*closo*-1,2-RhSB₉H₉] (14). The reaction was carried out with 100 mg (0.116 mmol) of 4, and the solution was exposed to an ethylene atmosphere for 4 h. Yield: 60 mg, 0.096 mmol, 83%. Anal. Calcd for C₂₆H₃₄B₉NPRhS: C, 50.06; H, 5.49; N, 2.5; S, 5.14. Found: C, 50.46; H, 5.66; N, 2.30; S, 5.08. IR (ATR, cm⁻¹): ν 2529 vs (BH), 2505 vs (BH), 2499 vs (BH), 2476 vs (BH), 2453 vs (BH), 1616 w, 1479 s, 1450 w, 1432 s, 1261 m, 1152 m, 1089 s, 1010 m, 947 m, 747 m, 692 s, 525 s, 491 m, 455 m (Rh-C₂H₄), 417 m (Rh-C₂H₄), 326 w (RhP). ¹H NMR (300 MHz, CD₂Cl₂, 300 K): δ 9.14 (m, 2H, 3-CH₃-NC₅H₄), 8.44 (m, 1H, 3-CH₃-NC₅H₄), 8.10 (m, 1H, 3-CH₃-NC₅H₄), 7.70–7.03 (15H, PPh₃), 2.52 (s, 3H, 3-CH₃-NC₅H₄), 2.28 (m, 2H, C₂H₄), 2.05 (m, 2H, C₂H₄). ³¹P{¹H} NMR (121 MHz, CD₂Cl₂, 300 K): δ 40.3 [d, $^1J_{\text{RHP}} = 137$ Hz, PPh₃]. LRMS (MALDI⁺/DCTB): m/z 595 [M - (C₂H₄) - H]⁺. Isotope envelopes match those calculated from the known isotopic abundances of the constituent elements.

[1,1-(PPh₃)₂(η²-C₂H₄)-3-(4-Me-NC₅H₄)-*closo*-1,2-RhSB₉H₉] (15). The reaction was carried out with 100 mg (0.116 mmol) of 5, and the solution was exposed to an ethylene atmosphere for 12 h. Yield: 54 mg, 0.087 mmol, 75%. Anal. Calcd for C₂₆H₃₄B₉NPRhS-CH₂Cl₂: C, 45.76; H, 5.12; N, 1.98; S, 4.52. Found: C, 45.91; H, 4.98; N, 1.69; S, 4.07. IR (ATR, cm⁻¹): ν 2549 vs (BH), 2517 vs (BH), 2482 vs (BH), 2470 vs (BH), 1630 s, 1478 m, 1451 w, 1433 s, 1256 w, 1161 m, 1090 s, 1005 s, 936 m, 743 s, 693 vs, 525 vs, 491 s, 457 m (Rh-C₂H₄), 424 m (Rh-C₂H₄), 339 w (RhP). ¹H NMR (300 MHz, CD₂Cl₂, 300 K): δ 9.14 (m, 2H, 4-CH₃-NC₅H₄), 7.53 (m, 2H, 4-CH₃-NC₅H₄), 7.70–7.01 (15H, PPh₃), 2.71 (s, 3H, 4-CH₃-NC₅H₄), 2.26 (m, 2H, C₂H₄), 2.06 (m, 2H, C₂H₄). ³¹P{¹H} NMR (121 MHz, CD₂Cl₂, 300 K): δ 40.3 [d, $^1J_{\text{RHP}} = 137$ Hz, PPh₃]. LRMS (MALDI⁺/DCTB): m/z 596 [M - (C₂H₄)]⁺. Isotope envelopes match those calculated from the known isotopic abundances of the constituent elements.

CO-Ligated *closo*-Rhodathioboranes 17–19. The procedure was the same as that for ethylene, but using a CO-filled balloon.

[1,1-(PPh₃)(CO)-3-(2-Me-NC₅H₄)-*closo*-1,2-RhSB₉H₉] (17). The reaction was carried out with 60 mg (0.070 mmol) of 3 with stirring under an atmosphere of CO for 2 h. Yield: 37.6 mg, 0.0604 mmol, 87%. Anal. Calcd for C₂₅H₃₀B₉NOPRhS-CH₂Cl₂: C, 44.06; H, 4.55; N, 1.98; S, 4.52. Found: C, 44.09; H, 4.53; N, 1.83; S, 4.27. IR (ATR,

cm⁻¹): ν 2567 vs (BH), 2520 vs (BH), 2493 vs (BH), 2466 vs (BH), 1982 vs (CO), 1632 m, 1479 m, 1434 m, 1262 m, 1161 m, 1092 m, 1006 m, 935 m, 935 m, 877 m, 829 m, 800 m, 746 m, 692 vs, 577 w, 525 vs. ¹H NMR (300 MHz, CD₂Cl₂, 300 K): δ 9.41 (d, 1H, 2-CH₃-NC₅H₄), 8.04 (d, 1H, 2-CH₃-NC₅H₄), 7.62 (t, 2H, 2-CH₃-NC₅H₄), 7.50–7.05 (15H, PPh₃), 3.02 (m, 3H, 2-CH₃-NC₅H₄). ³¹P{¹H} NMR (121 MHz, CD₂Cl₂, 300 K): δ 37.7 (d, $^1J_{\text{RHP}} = 133$ Hz; PPh₃). LRMS (MALDI⁺/DCTB): m/z 596 [M - (CO)]⁺. Isotope envelopes match those calculated from the known isotopic abundances of the constituent elements.

[1,1-(PPh₃)(CO)-3-(3-Me-NC₅H₄)-*closo*-1,2-RhSB₉H₉] (18). The reaction was carried out with 150 mg (0.174 mmol) of 4, and stirring under an atmosphere of CO was maintained for 2 h. Yield: 97.0 mg, 0.156 mmol, 90%. Anal. Calcd for C₂₅H₃₀B₉NOPRhS-CH₂Cl₂: C, 44.06; H, 4.55; N, 1.98; S, 4.52. Found: C, 44.41; H, 4.42; N, 1.76; S, 4.32. IR (ATR, cm⁻¹): ν 2563 vs (BH), 2519 vs (BH), 2494 vs (BH), 2464 vs (BH), 1974 vs (CO), 1619 m, 1478 m, 1433 m, 1180 m, 1093 m, 1005 m, 939 m, 742 m, 684 vs, 524 v. ¹H NMR (300 MHz, CD₂Cl₂, 300 K): δ 8.90 (d, 2H, 3-CH₃-NC₅H₄), 8.01 (d, 1H, 3-CH₃-NC₅H₄), 7.58 (t, 1H, 3-CH₃-NC₅H₄), 7.34–7.28 (15H, PPh₃), 2.40 (m, 3H, 3-CH₃-NC₅H₄). ³¹P{¹H} NMR (121 MHz, CD₂Cl₂, 300 K): δ 37.9 (d, $^1J_{\text{RHP}} = 136$ Hz; PPh₃). LRMS (MALDI⁺/DCTB): m/z 596 [M - (CO)]⁺. Isotope envelopes match those calculated from the known isotopic abundances of the constituent elements.

[1,1-(PPh₃)(CO)-3-(4-Me-NC₅H₄)-*closo*-1,2-RhSB₉H₉] (19). The reaction was carried out with 30 mg (0.035 mmol) of 5, and stirring under an atmosphere of CO was maintained for 8 h. Yield: 20.0 mg, 0.032 mmol, 91%. Anal. Calcd for C₂₅H₃₀B₉NOPRhS-CH₂Cl₂: C, 44.06; H, 4.55; N, 1.98; S, 4.52. Found: C, 44.51; H, 4.43; N, 1.73; S, 4.02. IR (ATR, cm⁻¹): ν 2567 vs (BH), 2523 vs (BH), 2501 vs (BH), 2465 vs (BH), 1993 vs (CO), 1978 vs (CO), 1632 m, 1479 m, 1452 w, 1434 m, 1163 m, 1092 s, 1006 m, 935 m, 746 s, 692 vs, 525 vs. ¹H NMR (300 MHz, CD₂Cl₂, 300 K): δ 8.97 (m, 2H, 4-CH₃-NC₅H₄), 7.46 (m, 2H, 4-CH₃-NC₅H₄), 7.36–7.27 (15H, PPh₃), 2.65 (s, 3H, 4-CH₃-NC₅H₄). ³¹P{¹H} NMR (121 MHz, CD₂Cl₂, 300 K): δ 37.9 (d, $^1J_{\text{RHP}} = 132$ Hz; PPh₃). LRMS (MALDI⁺/DCTB): m/z 596 [M - (CO)]⁺. Isotope envelopes match those calculated from the known isotopic abundances of the constituent elements.

Reactions with Carbon Monoxide: Characterization of Intermediates. Carbon monoxide was bubbled for several minutes (3–9 min) through a CD₂Cl₂ solution of the corresponding *nido*-hydridorhodathioborane 2–5 in a 5 mm NMR tube at room temperature. The sample was subsequently cooled to –50 °C in an isopropyl alcohol bath and transferred to an NMR spectrometer in which the temperature of the probe was set to –50 °C. The system was studied at different temperatures, allowing the identification of the different intermediates that form before hydrogen loss occurs to yield the CO ligated *closo* clusters 16–19 described above. The following are the NMR data for the reaction mixtures that contain the labile new species. Spectra can be seen in the main text as well the Supporting Information of this paper.

Reaction of 2 with CO. Nine minutes of CO bubbling. ¹H{¹B} NMR (500 MHz, CD₂Cl₂, 223 K): δ +9.27 to +7.06 (aromatics, NC₅H₅, PPh₃), +3.92 (s, BH), +3.41 (s, BH), +1.86 (s, BH), +0.28 (s, BH), –1.66 (low intensity br s, BH), –2.93 (s, BHB), –4.56 (s, BHB), –10.96 (low intensity apparent t, $^1J_{\text{RHH}} = 20.4$ Hz, RhH), –11.25 (d, $^1J_{\text{RHH}} = 22.1$ Hz, 1H). There are also resonances corresponding to 2, which is in solution as a minor species. ³¹P{¹H} NMR (202 MHz, CD₂Cl₂, 203 K): δ +38.9 (d, $^1J_{\text{RHP}} = 131$ Hz, compound 16), +36.6 (d, $^1J_{\text{RHP}} = 125.2$ Hz), +35.2 (d, $^1J_{\text{RHP}} = 99.4$ Hz), +29.5 (d, $^1J_{\text{RHP}} = 121.9$ Hz), +28.6 (O=PPh₃), –7.9 (PPh₃); the resonances exhibit a 1:2.94:11.30:1.60:0.77:14.04 relative intensity ratio, respectively. [¹H–³¹P]-HMBC (500 MHz, CD₂Cl₂, 203 K) {ordered as (δ_H, δ_P) correlation}: (–10.96, +29.5), (–11.35, +35.2); as expected, all the ³¹P resonances exhibit correlations with aromatic signals.

Reaction of 3 with CO. Three minutes of CO bubbling. ¹B{¹H} NMR (160 MHz, CD₂Cl₂, 273 K): δ +12.8 (s, minor species) +8.2 (d, $^1J_{\text{BH}} = 118$ Hz, major species), +5.8 (minor species), +3.6 (d, $^1J_{\text{BH}} = 72$ Hz, major), –2.1 (minor species), –4.4 (minor species), –9.2 (d, $^1J_{\text{BH}} = 137$ Hz, minor species), –13.5 (major species), –12.5 (minor

species), -13.5 (major species), -18.5 (minor species), -19.6 (d, $^1J_{\text{BH}} = 127$ Hz, major species), -22.3 (d, $^1J_{\text{BH}} = 146$ Hz, major species), -24.6 (major species), -26.0 (d, $^1J_{\text{BH}} = 146$ Hz, major species), -28.3 (d, $^1J_{\text{BH}} = 145$ Hz, minor species), -32.1 (minor species). $^1\text{H}\{^{11}\text{B}\}$ NMR (400 MHz, CD_2Cl_2 , 223 K): δ $+9.21$ (d, 5.2 Hz, *o*-2-Me- NC_5H_4 , minor species), $+9.15$ (d, 5.5 Hz, *o*-2-Me- NC_5H_4 , major species), $+7.98$ (pseudo-t, 7.5 Hz, 2-Me- NC_5H_4 , major species), $+7.92$ (pseudo-t, 7.5 Hz, 2-Me- NC_5H_4 , minor species), $+7.57$ to $+7.16$ (aromatics, 2-Me- NC_5H_4 , PPh_3), $+4.04$ (BH, minor species), $+3.37$ (BH, major species), $+3.03$ (BH, major), $+2.92$ (s, CH_3 ; minor species), $+2.60$ (BH, minor species), $+2.35$ (BH, major species), $+2.26$ (s, CH_3 ; major species), $+2.18$ (BH, major species), $+2.04$ (BH, minor species), $+1.87$ (BH, major species), $+1.32$ (2BH, major species), $+0.90$ (BH, minor species), $+0.15$ (BH, major species), -2.88 (s, BHB), -4.63 (s, BHB), -11.33 (d, $^1J_{\text{RhH}} = 22.3$ Hz, RhH). $^1\text{H}\{^{11}\text{B}\}$ NMR (400 MHz, CD_2Cl_2 , 273 K): selected resonances, -2.81 (s, BHB), -4.59 (s, BHB), -11.42 (d, $^1J_{\text{RhH}} = 17.8$ Hz, RhH), relative intensity ratio 1:1:0.27. $^{31}\text{P}\{^1\text{H}\}$ NMR (162 MHz, CD_2Cl_2 , 223 K): δ $+35.5$ (d, $^1J_{\text{RHP}} = 127$ Hz), $+35.0$ (br. d, $^1J_{\text{RHP}} = 91$ Hz; this broad signal overlaps partially with the previous resonance), $+28.4$ (O= PPh_3), -7.4 (PPh_3): the resonances exhibit a 2.0:0.7:0.4:2.3 relative intensity ratio, respectively. [$^1\text{H}-^{31}\text{P}$]-HMBC (500 MHz, CD_2Cl_2 , 203 K) {ordered as (δ_{H} , δ_{P}) correlation}: [-11.28 , $+35.7$ (br peak)]. [$^1\text{H}-^1\text{H}$]-NOESY (500 MHz, CD_2Cl_2 , 273 K): (-2.75 , -11.31); this off-diagonal peak is of the same phase as the diagonal peaks, demonstrating that the correlation is due to chemical exchange between the Rh-H hydride ligand and the B-H-B bridging hydrogen atom of one of the intermediates.

Reaction of 4 with CO. $^1\text{H}\{^{11}\text{B}\}$ NMR (400 MHz, CD_2Cl_2 , 223 K): δ $+8.97$ (m, 3-Me- NC_5H_4 , minor), $+8.88$ (m, 3-Me- NC_5H_4 , major), $+8.75$ (s, 3-Me- NC_5H_4 , major), $+8.65$ (s, 3-Me- NC_5H_4 , major), $+7.65$ to $+6.71$ (aromatics, 4-Me- NC_5H_4 and PPh_3), $+3.95$ (s, BH, major), $+3.50$ (s, BH, major), $+2.99$ (s, BH, minor), $+2.11$ (s, CH_3), $+1.99$ (s, BH, major), $+1.39$ (s, BH, major), $+1.29$ (s, BH), $+1.05$ (s, BH), $+0.89$ (s, BH), $+0.24$ (s, BH), -1.60 (BH, minor species), -2.99 (s, BHB), -4.55 (s, BHB), -10.88 (low intensity apparent t, $J = 10.88$ Hz, RhH), -11.86 (d, $^1J_{\text{RhH}} = 22.6$ Hz, RhH).

Reaction of 5 with CO. $^{11}\text{B}\{^1\text{H}\}$ NMR (160 MHz, CD_2Cl_2 , 273 K): δ $+55.2$ (compound 19), $+27.9$ (compound 19), $+15.9$, $+8.17$, $+7.0$, $+5.0$ ($^1J_{\text{BH}} = 119$ Hz), $+1.2$, -3.1 , -9.8 ($^1J_{\text{BH}} = 145$ Hz), -13.5 , -19.3 , -20.3 , -22.8 (compound 19), -25.2 ($^1J_{\text{BH}} = 132$ Hz), -28.2 ($^1J_{\text{BH}} = 145$ Hz), -32.5 (compound 19). $^1\text{H}\{^{11}\text{B}\}$ NMR (500 MHz, CD_2Cl_2 , 223 K): δ $+8.84$ (br. m, 4-Me- NC_5H_4), $+8.67$ (d, $J = 6.0$ Hz, 4-Me- NC_5H_4), $+7.65$ to $+6.71$ (aromatics, 4-Me- NC_5H_4 and PPh_3), $+3.90$ (s, BH), $+3.39$ (s, BH), $+2.57$ (s, BH), $+2.11$ (s, CH_3), $+1.96$ (s, BH), $+1.37$ (s, BH), $+1.29$ (s, BH), $+1.05$ (s, BH), $+0.89$ (s, BH), $+0.24$ (s, BH), -1.64 (BH, minor species), -2.99 (s, BHB), -4.55 (s, BHB), -10.95 (low intensity apparent t, $J = 19.9$ Hz, RhH), -11.26 (d, $^1J_{\text{RhH}} = 22.6$ Hz, RhH). $^1\text{H}\{^{11}\text{B}\}$ NMR (500 MHz, CD_2Cl_2 , 300 K): δ $+9.18$ to $+6.38$ (aromatics, 4-Me- NC_5H_4 and PPh_3), $+3.82$ (BH), $+3.40$ (BH), $+3.04$ (BH), $+2.65$ (BH), $+2.51$ (s, CH_3 ; major component), $+2.30$ (BH), $+2.24$ (BH), $+2.11$ (s, CH_3 ; minor component), $+1.45$ (BH), $+1.28$ (BH), $+1.02$ (BH), $+0.21$ (BH), -2.92 (v broad, BHB), -4.51 (v. broad, BHB), -10.96 (apparent triplet, $J_{\text{RhH}} = 22.9$ Hz, minor species), -11.35 (d, $^1J_{\text{RhH}} = 21.3$ Hz, RhH); there are also resonances corresponding to 19, which is in solution as a minor species. $^{31}\text{P}\{^1\text{H}\}$ NMR (121 MHz, CD_2Cl_2 , 223 K): δ $+38.6$ (d, $^1J_{\text{RHP}} = 131$ Hz, compound 19), $+36.6$ (d, $^1J_{\text{RHP}} = 125$ Hz), $+34.5$ (d, $^1J_{\text{RHP}} = 103$ Hz), $+29.8$ (d, $^1J_{\text{RHP}} = 122$ Hz), $+28.4$ (O= PPh_3), -7.4 (free PPh_3): the resonances exhibit a 1.00:1.90:9.86:0.76:0.28:11.50 relative intensity ratio, respectively. $^{31}\text{P}\{^1\text{H}\}$ NMR (121 MHz, CD_2Cl_2 , 300 K): δ $+37.8$ (d, $^1J_{\text{RHP}} = 126$ Hz, compound 19) $+35.8$ (very broad, PPh_3), $+32.8$ (very broad, PPh_3), $+27.2$ (O= PPh_3), -5.3 (free PPh_3): the resonances exhibit a 1.00:0.24:0.33:0.04:1.02 relative intensity ratio, respectively. [$^1\text{H}-^{31}\text{P}$]-HMBC (500 MHz, CD_2Cl_2 , 223 K) {ordered as (δ_{H} , δ_{P}) correlation}: (-10.95 , $+29.8$), (-11.35 , $+34.5$), ($+2.65$, $+34.5$); as expected, all the ^{31}P resonances correlate with aromatic signals.

Reactions with Alkenes. $[8,8,8\text{-H}(\text{PPh}_3)_2\text{-9}(\text{NC}_5\text{H}_5)\text{-nido-8,7-RHSB}_9\text{H}_9]$ (2) with Cyclohexene. Two milligrams (0.0025 mmol) of

2 and a 20-fold excess of cyclohexene were stirred for 7 days with no sign of reaction.

$[8,8,8\text{-H}(\text{PPh}_3)_2\text{-9}(\text{NC}_5\text{H}_5)\text{-nido-8,7-RHSB}_9\text{H}_9]$ (2) with 1-Hexene. In a 5 mm NMR tube, 2 mg (0.0025 mmol) of 2 was dissolved in 0.6 mL of CH_2Cl_2 together with a 20-fold excess of 1-hexene. GC after 1 day of reaction showed a mixture of 1-hexene (75%), 2-hexene (17%), 3-hexene (7%), and hexane (1%).

$[8,8,8\text{-H}(\text{PPh}_3)_2\text{-9}(\text{NC}_5\text{H}_5)\text{-nido-8,7-RHSB}_9\text{H}_9]$ (2) with Propylene. In a 5 mm NMR tube, 16 mg (0.018 mmol) of 2 was dissolved in 0.6 mL of CD_2Cl_2 in a NMR tube and propylene was bubbled through the solution for 5 min. After 4 days of stirring, the composition of the reaction mixture contained propylene, some propane, *closo* derivative 8 (65%), and starting material 2 (35%).

$[8,8,8\text{-H}(\text{PPh}_3)_2\text{-9}(2\text{-Me-NC}_5\text{H}_4)\text{-nido-8,7-RHSB}_9\text{H}_9]$ (3) with Cyclohexene. In a 5 mm NMR tube, 12.5 mg (0.014 mmol) of 3 in 0.6 mL of CD_2Cl_2 and a 20-fold excess of cyclohexene were dissolved. After 5 days, there was formation of cyclohexane (2%) and the *closo*-rhodathiaborane 9.

$[8,8,8\text{-H}(\text{PPh}_3)_2\text{-9}(2\text{-Me-NC}_5\text{H}_4)\text{-nido-8,7-RHSB}_9\text{H}_9]$ (3) with 1-Hexene. In a Schlenk tube, 12.5 mg (0.014 mmol) of 3 was dissolved in 0.6 mL of CH_2Cl_2 with a 20-fold excess of 1-hexene. The solution was stirred at room temperature under an atmosphere of argon. The reaction was monitored by GC, and after 1 day the composition of the mixture was 34% of 2-hexene, 63% of 1-hexene, and 3% of hexane. Compound 3 afforded the *closo* derivative 9.

$[8,8,8\text{-H}(\text{PPh}_3)_2\text{-9}(2\text{-Me-NC}_5\text{H}_4)\text{-nido-8,7-RHSB}_9\text{H}_9]$ (3) with Propylene. In an NMR tube, 14 mg (0.016 mmol) of 3 was dissolved in 0.6 mL of CD_2Cl_2 and propylene gas was bubbled through the solution for 5 min. In 1 h, the hydridorhodathiaborane underwent transformation to the *closo* cluster 9, with concomitant formation of propane.

■ ASSOCIATED CONTENT

📄 Supporting Information

Figures, tables, and CIF files giving 1D and 2D NMR spectra, DFT-calculated coordinates and energies, and crystallographic data for 4, 5, and 9. This material is available free of charge via the Internet at <http://pubs.acs.org>.

■ AUTHOR INFORMATION

✉ Corresponding Author

*E-mail for R.M.: rmacias@unizar.es.

Notes

The authors declare no competing financial interest.

■ ACKNOWLEDGMENTS

We acknowledge the Spanish Ministry of Science and Innovation (CTQ2009-10132, CONSOLIDER INGENIO, CSD2009-00050, MULTICAT and CSD2006-0015, Crystallization Factory) for support of this work. B.C. thanks the "Diputación General de Aragón" for a predoctoral scholarship. We also thank Dr. J. Bould for useful discussions.

■ REFERENCES

- (1) (a) Grimes, R. N. In *Comprehensive Organometallic Chemistry*; Wilkinson, G., Stone, F. G. A., Abel, E. W., Eds.; Pergamon Press: Oxford, U.K., 1982; Vol. 1. (b) Grimes, R. In *Metal Interactions with Boron Clusters*; Grimes, R., Ed.; Springer: New York, 1982. (c) Grimes, R. N. *Chem. Rev.* **1992**, *92*, 251. (d) Grimes, R. N. In *Comprehensive Organometallic Chemistry II*; Abel, E. W., Stone, F. G. A., Wilkinson, G., Eds.; Pergamon: Oxford, U.K., 1995; Vol. 1. (f) Hodson, B. E.; McGrath, T. D.; Stone, F. G. A. *Organometallics* **2005**, *24*, 1638. (g) McGrath, T. D.; Stone, F. G. A. *J. Organomet. Chem.* **2004**, *689*, 3891. (h) Ellis, D. D.; Jelliss, P. A.; Stone, F. G. A. *Spec. Publ. - R. Soc. Chem.* **2000**, *253*, 291. (i) Jelliss, P. A.; Stone, F. G. A. *J. Organomet. Chem.* **1995**, *500*, 307. (j) Brew, S. A.; Stone, F. G. A. *Adv. Organomet. Chem.* **1993**, *35*, 135. (k) Stone, F. G. A. *Adv. Organomet. Chem.* **1990**,

- 31, 53. (l) Saxena, A. K.; Maguire, J. A.; Hosmane, N. S. *Chem. Rev.* **1997**, *97*, 2421. (m) Saxena, A. K.; Hosmane, N. S. *Chem. Rev.* **1993**, *93*, 1081. (e) McGrath, T. D.; Stone, F. G. A. *Adv. Organomet. Chem.* **2005**, *53*, 1.
- (2) (a) Kennedy, J. D. *Prog. Inorg. Chem.* **1986**, *34*, 211. (b) Kennedy, J. D. *Prog. Inorg. Chem.* **1984**, *32*, 519. (c) Barton, L., Strivastava, D. K. In *Comprehensive Organometallic Chemistry II*; Abel, E. W., Stone, F. G. A., Wilkinson, G., Eds.; Pergamon: New York, 1995; Vol. 1. (d) Todd, L. T. In *Comprehensive Organometallic Chemistry II*; Abel, E. W., Stone, F. G. A., Wilkinson, G., Eds.; Elsevier Science: Oxford, U.K., 1995; Vol. 1. (e) Todd, L. T. In *Comprehensive Organometallic Chemistry*; Wilkinson, G., Stone, F. G. A., Abel, E. W., Eds.; Pergamon Press: Oxford, U.K., 1982; Vol. 1. (f) Wesemann, L. In *Comprehensive Organometallic Chemistry*; Mingos, D. M. P., Crabtree, R. H., Eds.; Elsevier: Oxford, U.K., 2007; Vol. 3. (g) Weller, A. S. In *Comprehensive Organometallic Chemistry III*; Crabtree, R. H., Mingos, D. M. P., Eds.; Elsevier: Oxford, U.K., 2007; Vol. 3.
- (3) (a) Wade, K. *Adv. Inorg. Chem. Radiochem.* **1976**, *18*, 1. (b) Williams, R. E. *Adv. Inorg. Chem. Radiochem.* **1976**, *18*, 67.
- (4) Ferguson, G.; Jennings, M. C.; Lough, A. J.; Coughlan, S.; Spalding, T. R.; Kennedy, J. D.; Fontaine, X. L. R.; Stibr, B. *J. Chem. Soc., Chem. Commun.* **1990**, 891.
- (5) Calvo, B.; Kess, M.; Macías, R.; Cunchillos, C.; Lahoz, F. J.; Kennedy, J. D.; Oro, L. A. *Dalton Trans.* **2011**, *40*, 6555.
- (6) (a) Álvarez, Á.; Macías, R.; Fabra, M. J.; Lahoz, F. J.; Oro, L. A. *J. Am. Chem. Soc.* **2008**, *130*, 2148. (b) Álvarez, Á.; Macías, R.; Bould, J.; Fabra, M. J.; Lahoz, F. J.; Oro, L. A. *J. Am. Chem. Soc.* **2008**, *130*, 11455.
- (7) Calvo, B.; Macías, R.; Polo, V.; Artigas, M. J.; Lahoz, F. J.; Oro, L. A. *Chem. Commun.* **2013**, *49*, 9863.
- (8) Calvo, B.; Macías, R.; Artigas, M. J.; Lahoz, F. J.; Oro, L. A. *Dalton Trans.* **2014**, *43*, S121.
- (9) Calvo, B.; Álvarez, Á.; Macías, R.; García-Orduña, P.; Lahoz, F. J.; Oro, L. A. *Organometallics* **2012**, *31*, 2986.
- (10) Álvarez, Á.; Macías, R.; Bould, J.; Cunchillos, C.; Lahoz, F. J.; Oro, L. A. *Chem. Eur. J.* **2009**, *15*, 5428.
- (11) Calvo, B.; Macías, R.; Artigas, M. J.; Lahoz, F. J.; Oro, L. A. *Chem. Eur. J.* **2013**, *19*, 3905.
- (12) Calvo, B.; Macías, R.; Artigas, M. J.; Lahoz, F. J.; Oro, L. A. *Inorg. Chem.* **2012**, *52*, 211.
- (13) (a) Macías, R.; Bould, J.; Holub, J.; Kennedy, J. D.; Štibr, B.; Thornton-Pett, M. *Dalton Trans.* **2007**, 2885. (b) Bould, J.; Macías, R. *J. Organomet. Chem.* **2014**, *761*, 120.
- (14) McAnaw, A.; Scott, G.; Elrick, L.; Rosair, G. M.; Welch, A. J. *Dalton Trans.* **2013**, *42*, 645.
- (15) (a) Macías, R.; Holub, J.; Kennedy, J. D.; Štibr, B.; Thornton-Pett, M. *J. Chem. Soc., Chem. Commun.* **1994**, 2265. (b) Nestor, K.; Kennedy, J. D.; Thornton-Pett, M.; Holub, J.; Štibr, B. *Inorg. Chem.* **1992**, *31*, 3339. (c) Bould, J.; Rath, N. P.; Barton, L. *Organometallics* **1996**, *15*, 4916.
- (16) Bould, J.; Cunchillos, C.; Lahoz, F. J.; Oro, L. A.; Kennedy, J. D.; Macías, R. *Inorg. Chem.* **2010**, *49*, 7353.
- (17) Beall, H.; Bushweller, C. H.; Dewkett, W. J.; Grace, M. *J. Am. Chem. Soc.* **1970**, *92*, 3484.
- (18) Merrick, J. P.; Moran, D.; Radom, L. *J. Phys. Chem. A* **2007**, *111*, 11683.
- (19) Kononova, E. G.; Leites, L. A.; Bukalov, S. S.; Pisareva, I. V.; Chizhevsky, I. T.; Kennedy, J. D.; Bould, J. *Eur. J. Inorg. Chem.* **2007**, 4911.
- (20) (a) Nestor, K.; Fontaine, X. L. R.; Greenwood, N. N.; Kennedy, J. D.; Plešek, J.; Štibr, B.; Thornton-Pett, M. *Inorg. Chem.* **1989**, *28*, 2219. (b) Bown, M.; Fontaine, X. L. R.; Greenwood, N. N.; Kennedy, J. D.; Thornton-Pett, M. *Organometallics* **1987**, *6*, 2254. (c) Nestor, K.; Fontaine, X. L. R.; Greenwood, N. N.; Kennedy, J. D.; Thornton-Pett, M. *J. Chem. Soc., Chem. Commun.* **1989**, 455.
- (21) Volkov, O.; Radacki, K.; Thomas, R. L.; Rath, N. P.; Barton, L. *J. Organomet. Chem.* **2005**, *690*, 2736.
- (22) Balagurova, E. V.; Cheredilin, D. N.; Kolomnikova, G. D.; Tok, O. L.; Dolgushin, F. M.; Yanovsky, A. I.; Chizhevsky, I. T. *J. Am. Chem. Soc.* **2007**, *129*, 3745.
- (23) (a) Long, J. A.; Marder, T. B.; Behnken, P. E.; Hawthorne, M. F. *J. Am. Chem. Soc.* **1984**, *106*, 2979. (b) Ellis, D. D.; Franken, A.; Jelliss, P. A.; Kautz, J. A.; Stone, F. G. A.; Yu, P.-Y. *J. Chem. Soc., Dalton Trans.* **2000**, 2509. (c) Pisareva, I. V.; Konoplev, V. E.; Petrovskii, P. V.; Vorontsov, E. V.; Dolgushin, F. M.; Yanovsky, A. I.; Chizhevsky, I. T. *Inorg. Chem.* **2004**, *43*, 6228.
- (24) (a) Hawthorne, M. F.; Ramachandran, B. M.; Kennedy, R. D.; Knobler, C. B. *Pure Appl. Chem.* **2006**, *78*, 1299. (b) Oconnell, D.; Patterson, J. C.; Spalding, T. R.; Ferguson, G.; Gallagher, J. F.; Li, Y. W.; Kennedy, J. D.; Macías, R.; Thornton-Pett, M.; Holub, J. *J. Chem. Soc., Dalton Trans.* **1996**, 3323. (c) Macías, R.; Thornton-Pett, M.; Holub, J.; Spalding, T. R.; Faridoun, Y.; Štibr, B.; Kennedy, J. D. *J. Organomet. Chem.* **2008**, *693*, 435.
- (25) Fontaine, X. L. R.; Kennedy, J. D. *J. Chem. Soc., Dalton Trans.* **1987**, 1573.
- (26) Keeler, J. *Understanding NMR Spectroscopy*; Wiley: Chichester, U.K., 2010.
- (27) Henderson, W.; McIndoe, J. S. *Mass Spectrometry of Inorganic and Organometallic Compounds*, 2005 ed.; Wiley: Chichester, U.K., 2005.
- (28) Otwinowski, Z.; Minor, W. In *Methods in Enzymology*; Carter, C. W., Ed.; Academic Press: New York, 1997; Vol. 276.
- (29) Blessing, R. H. *Acta Crystallogr., Sect. A* **1995**, *A51*, 33.
- (30) Sheldrick, G. M. *SHELXS-86*; University of Göttingen, Göttingen, Germany, 1997.
- (31) Sheldrick, G. M. *Acta Crystallogr., Sect. A* **2008**, *A64*, 112.
- (32) Frisch, M. J.; Trucks, G. W.; Schlegel, H. B.; Scuseria, G. E.; Robb, M. A.; Cheeseman, J. R.; Scalmani, G.; Barone, V.; Mennucci, B.; Petersson, G. A.; Nakatsuji, H.; Caricato, M.; Li, X.; Hratchian, H. P.; Izmaylov, A. F.; Bloino, J.; Zheng, G.; Sonnenberg, J. L.; Hada, M.; Ehara, M.; Toyota, K.; Fukuda, R.; Hasegawa, J.; Ishida, M.; Nakajima, T.; Honda, Y.; Kitao, O.; Nakai, H.; Vreven, T.; Montgomery, J. A., Jr.; Ogliaro, F.; Bearpark, M.; Heyd, J. J.; Brothers, E.; Kudin, K. N.; Staroverov, V. N.; Kobayashi, R.; Normand, J.; Raghavachari, K.; Rendell, A.; Burant, J. C.; Iyengar, S. S.; Tomasi, J.; Cossi, M.; Rega, N.; Millam, J. M.; Klene, M.; Knox, J. E.; Cross, J. B.; Bakken, V.; Adamo, C.; Jaramillo, J.; Gomperts, R.; Stratmann, R. E.; Yazyev, O.; Austin, A. J.; Cammi, R.; Pomelli, C.; Ochterski, J. W.; Martin, R. L.; Morokuma, K.; Zakrzewski, V. G.; Voth, G. A.; Salvador, P.; Dannenberg, J. J.; Dapprich, S.; Daniels, A. D.; Farkas, Ö.; Foresman, J. B.; Ortiz, J. V.; Cioslowski, J.; Fox, D. J. *Gaussian 09*; Gaussian, Inc., Wallingford, CT, 2009.